Odor Modulation of Electrical and $[Ca^{2+}]_i$ Activities in Neurons of the Olfactory Bulb

PhD Thesis

in partial fulfilment of the requirements
for the degree “Doctor of Philosophy (PhD)/Dr. rer. nat.”
in the Neuroscience Program
at the Georg August University Göttingen,
Faculty of Biology

submitted by

Bei-Jung Lin

……

born in

Taipei, Taiwan

……

2006

Adivsor, member of PhD committee: Prof. Dr. Dr. Detlev Schild
Member of PhD committee: Prof. Dr. Eberhard Fuchs
Member of PhD committee: Prof. Dr. Walter Stuehmer

Date of submission of the PhD Thesis: March 21th, 2006

Herewith I declare, that I prepared the PhD Thesis
'Odor Modulation of Electrical and $[Ca^{2+}]_i$ Activities in Neurons of the Olfactory Bulb.'
independently and with no other sources and aids than quoted

…….

1. Introduction

The ability to detect chemical signals in the environment is crucial for many organisms. From insects to mammals, from aquatic to terrestrial animals, a wide variety of species rely on olfaction to locate food, to detect predators, and to find their mates (Bruce, 1959; Chivers *et al.*, 2001; Pearl *et al.*, 2000). Although appreciated by few people, the olfactory sense also profoundly influences human behaviors, especially through the induction of various emotions. For example, human's preference to an object can be dramatically reverted by replacing its pleasant odor with an unpleasant odor. (Imagine if a delicious cake smells like garbage!) Moreover, people who lose their olfaction often report a much more severe deterioration in their life quality than expected. These prevailing influences have motivated researchers from many different disciplines to search for principles of olfactory perception.

1.1 The olfactory system

Olfactory systems of most animals commonly face a formidable task, i.e. to recognize a large repertoire of natural odors consisting of mixtures of many chemicals in a turbulent air or water flow with noisy molecular background. Although the number of natural occurring odors is staggeringly large, odors that can be recognized doesn't seem to be limited by this number. Many randomly synthesized odors can be perceived as distinct and meaningful. Thus, the size of recognizable 'odor space' might keep growing as more possibilities are tested. In addition to the ability of sensing a large number of odorant molecules, animals can both discriminate the presence of a weak

odor in a noisy background and orientate themselves according to the fluctuating odorant signal towards a far away source. To achieve these, olfactory systems have to adapt highly optimized strategies to cope with these challenges.

Despite widely varying body plans and living environments, the olfactory systems in different animals share some surprising morphological similarities. For example, the olfactory receptor neuron in most species shows a similar bipolar structure with ciliary dendritic terminals (Ache & Young, 2005). Moreover, the axons of olfactory receptor neurons contact the dendrites of secondary neurons in prominent spherical neuropiles called glomeruli**,** a structure that can be found in the olfactory system of animals as different as humans and flies. Considering the long history of olfactory evolution, such conserved organization suggests that they may provide considerable functional advantages. Understanding the common principles underlying the unique abilities of olfaction has been one of the central themes of the olfactory research.

1.2 Odorants are detected by the receptor neurons

Odor perception starts at the cilia of receptor neurons where the binding between odorant molecules and olfactory receptor proteins takes place. Such binding induces a transduction cascade that leads to a depolarization and the firing of action potentials. The spiking information is then conveyed through the olfactory nerve to the olfactory bulb, the first brain region that receives odor information.

The olfactory receptors belong to a large family of G-protein coupled receptors (Dohlman *et al.*, 1991). There are ~1000 different genes in mouse

and ~500-750 different genes in human that encode olfactory receptor proteins (Ressler *et al.*, 1994a). Odorant molecules are recognized by the receptor proteins in a combinatorial manner (Breer, 2003), that is, each receptor can recognize many different odorant molecules and each odor is recognized by multiple olfactory receptors.

1.3 The olfactory bulb

The olfactory bulbs are spherical structures located at the frontal part of the brain. Different from the cerebral cortex, the olfactory bulbs have only two cell layers (the mitral and granule cell layer) and several layers formed by interconnecting neuropiles (the glomerulus layer, the internal plexiform layer, and the external plexiform layer).

Compared to other sensory systems, the olfactory system is structurally shallow in the sense that only one intermediate layer—the olfactory bulb—separates olfactory sensory neurons from cortex (Laurent, 1999). Unlike the retina, where the information between sensory neurons extensively interacts through two stages of lateral connections before sending it to the brain, there are no known synaptic interactions between olfactory receptor neurons in the olfactory epithelium. After olfactory bulb, the odorant information is then project diffusely into many different brain regions including the amygdale, the piriform cortex and the entorhinal cortex. Thus, olfactory bulb is not only the first stage of odor information processing but also the last stage before the information diverges. Any fundamental and common odor processing events must take place in this region; otherwise they will have to be implemented twice. For these reasons, the olfactory bulb is one of the major focuses of olfactory research and is also the main subject of this study. In the following,

we give a detailed introduction to the major anatomical organization of the olfactory bulb.

1.3.1 Glomeruli

When axons of the olfactory receptor neurons enter the olfactory bulb, they form synapses with dendritic terminals of projecting neurons as well as some local interneurons. These synapses and processes aggregate into many separated, neuropile-rich spheroid termed glomeruli. Given the fact that there are much fewer glomeruli than the receptor neurons, there is a prominent convergence from receptor neurons to individual glomerulous. It has been shown that the axons of the subset of receptor neurons expressing the same olfactory receptor gene converge to a small subset of glomeruli (Russler *et al.* 1994b; Vassar *et al.*, 1994). Through such a specific convergence, glomeruli may serve to collect and transform signals from receptor neurons into a patterned input to projecting neurons.

1.3.2 Mitral cells

Beneath the glomerulus layer, the olfactory bulb contains a layer of relay neurons that are responsible for conveying odor information to higher brain centers. These cells are termed ‘mitral cells’ in vertebrates based on their morphological characteristics or simply ‘projecting neurons’ in the olfactory system of insects.

In addition to the thick primary dendrites receiving input from individual glomeruli, mitral cells also possess secondary dendrites which receive bulbar inhibitory input. Typically, dendrites of projecting neurons receive synaptic

inputs while axons convey the output by propagating action potentials and releasing neurotransmitters. However, there exist presynaptic and postsynaptic machineries on mitral cell dendrites that can both release neurotransmitters and receive synaptic inputs. Many studies have confirmed the active property of mitral cell dendrites and their abilities to propagate action potentials in backward direction (i.e. from soma to dendrite). The back-propagation of action potential can act as triggers for dendritic transmitter release (Bischofberge & Jonas, 1997; Chen *et al.*, 1997). Moreover, such dendritic AP propagation can be modulated by the inhibitory system along the dendrites (Lowe, 2002; Xiong & Chen, 2002). These findings suggest that the signal processing events carried out by a single mitral cell may be highly complex.

1.3.3 Granule cells

Granule cells are GABAergic interneurons located in the deepest layer of the olfactory bulb. These neurons show spiny dendrites extending toward the mitral cell layer and make reciprocal synaptic contacts with the dendrites of mitral cells. Generally, granule cells do not have axons (Shepherd, 1972). Thus, both input and output of granule cells take place at their dendrites.

The dendrodendritic reciprocal connection between mitral cell dendrite and granule cell spine is one of the major characteristics of bulbar circuitry. Glutamate released from mitral cell dendrites activates NMDA receptors in granule cell spines, which leads to calcium influx and exocytosis of GABA back onto the same MC (Shipley & Ennis, 1996). Such reciprocal connection provides a fast and powerful mechanism for MC to inhibit itself, which may contribute to sharpening the response of MCs to specific odors.

1.4 Characterizing systems activity in the olfactory bulb

1.4.1 The experimental model

To characterize function of a sensory nervous system, one would like to correlate the systems activity with defined sensory stimuli. On the other hand, in vitro preparation permits the investigation of the detailed mechanisms underlying the observed stimulus activity. To do both, it requires an in vitro experimental system including the peripheral sensory cells that allow the system to 'sense' stimuli. However, due to an anatomical interruption between the olfactory epithelium and the olfactory bulb, preparing isolated recording system containing both organs from mammals encounters unmanageable difficulty.

In contrast, making such preparation from tadpoles is feasible. Using this preparation, one can characterize the stimulus activity of the olfactory bulb and further investigate the mechanisms underlying the bulbar activity.

1.4.2 Patterns of systems activity

Compared to visual and auditory sense, olfaction is regarded as a slowly evolving sense, thereby allowing sensory information to be coded in time. It has been shown in *in-vivo* electrophysiological recordings that mitral cells exhibit various dynamic odor-evoked electrical responses with both excitatory and inhibitory components suggesting temporal patterns of stimulus activity may code odorant information (Kauer, 1974; Friedrich & Laurent, 2001; Cang & Isaacson, 2003; Lin *et al.*, 2005).

On the other hand, functional imaging has revealed that odorants elicit

localized spatial patterns of active glomerular modules (Friedrich & Korsching 1997, Wong *et al.*, 2002). Specific spatial patterns of responsive mitral cells may be a way of representing spatial info-rich inputs. Lateral and recurrent inhibition, as suggested by intrabulbar circuitry, may further shape the pattern unique to different odorant stimulation. Thus, all these thoughts motivate us to study the spatial distribution patterns of the responsive mitral cells.

1.4.3 Multi-neuronal recordings using calcium imaging

Monitoring activities of neuronal population is required for investigating systems activity, especially when the spatial patterning is concerned. Over the last decade, calcium imaging with multi-cell staining has emerged as one of the most widespread techniques for recording many neurons simultaneously. Superb spatial resolution with defined contours of individual cells in calcium imaging enables discrimination of activities in adjacent cells, which is difficult to achieve by any previous methods (Ohki *et al.*, 2005). In addition, calcium imaging allows sampling of hundreds of neuronal cell bodies in parallel (Yuste and Katz, 1991; Yuste *et al.*, 1992). The powerful sampling ability is potentially useful for investigating dense and compact vertebrate nervous systems. Studies using calcium imaging have shown important functional properties in visual (Ohki *et al.*, 2005), barrel (Stosiek *et al.*, 2003) and frontal (Ikegaya *et al.*, 2004) cortexes, which are not accessible by previous electrophysiological recordings.

1.4.4 Relating $[Ca^{2+}]_i$ to the electrical activity

As action potentials activate voltage-activated calcium channels (VACCs)

thereby leading to influxes of calcium ions, it is generally believed that the occurrence of action potentials is accompanied by increase of somatic $[Ca^{2+}]_i$. Many laboratories have thus used $[Ca^{2+}]_i$ to establish neuronal activity implicitly assuming that neuronal activity and $[Ca^{2+}]_i$ are correlated (Mao *et al.*, 2001; Ohki *et al.*, 2005; Sullivan *et al.*, 2005; Czesnik *et al.*, 2003).

However, $[Ca^{2+}]_i$ could also be regulated by processes that are not related to action potentials such as activation of low-voltage-activated T-type calcium channels by subthreshold depolarization, activation of calcium-permeable neurotransmitter receptors (Kovalchuk *et al.*, 2000) and calcium release from the endoplasmatic reticulum (Kuba *et al.*, 1992). Moreover, increasing $[Ca^{2+}]_i$ may inactivate the VACCs (Kramer and Zucker, 1985; Adams and Levitan, 1985) or activate potassium and chloride channels (Hille, 2001; Yumada *et al.*, 2004); thereby reduce the excitability of neurons or inhibit spikes. Thus, the degree of correlation between somatic $[Ca^{2+}]_i$ and APs may depend on the $[Ca^{2+}]_i$ handling machinery expressed in a specific compartment of a specific cell type.

While most calcium imaging data show a stereotyped calcium increasing waveform implicitly referred as neuronal excitation (Wang *et al.*, 2004; Carlsson *et al.*, 2005), it raises a question that how the inhibitory and dynamic electrical responses, like neurons in the olfactory bulb show, are reflected in their calcium waveforms. On the other hand, the relationship between the sensory evoked somatic calcium responses and neuronal spike activity is still unclear, and neither has it been studied in various types of sensory neurons. Despite a number of studies examining the relationship between $[Ca^{2+}]_i$ and action potentials by intracellularly injecting constant current to evoke spikes (Smetters *et al.*, 1999; Waters *et al.*, 2003), the $[Ca^{2+}]_i$ responses could be different as cells are activated by direct current injection or by sensory

stimulation through a network. It thus remains to be shown whether a sensory driven $[Ca^{2+}]_i$ response faithfully reflects neuronal action potentials, or to what degree one activity is correlated with the other.

1.5 Goal of the thesis

In this these, neuronal spiking activity of olfactory bulb neurons is first characterized in a novel nose-OB slice preparation from tadpoles of *Xenopus laevis*. Because this preparation specially allows the investigation of the mechanisms underlying odorant-induced response in olfactory bulb neurons, we thus ask what subthreshold membrane potential responses and synaptic currents would occur in the bulbar neurons when the odorant information is processed in the olfactory bulb.

Second, to monitor activity of neuronal population in the olfactory bulb, we apply calcium imaging to record somatic $[Ca^{2+}]_i$ dynamics in a large number of single bulbar neurons. $[Ca^{2+}]_i$ responses to odorant stimulation are investigated in individual neurons as well as in neuron ensembles to reveal both temporal and spatial response patterns.

Third, in order to interpret the somatic $[Ca^{2+}]_i$ activity as the neuronal spiking activity, we simultaneously record $[Ca^{2+}]_i$ and spikes from individual neurons and establish the degree of correlation between these two signals.

2. Material and Methods

2.1 Nose-olfactory bulb preparation

Tadpoles of *Xenopus laevis* (stage 50-54; Nieuwkoop and Faber, 1956) were anaesthetized in a mixture of ice and water. A block of tissue containing the olfactory mucosae, the olfactory nerves and the rostral part of the brain (Fig. 2.1) was isolated and kept in the frog Ringer's solution containing 98 mM NaCl, 2 mM KCl, 1 mM $MgCl_2$, 5 mM glucose, 5 mM Na-pyruvate, 10 mM HEPES (230 mOsm, pH 7.8; Sigma). The dorsal part of the olfactory bulb was horizontally sliced off using a vibrotome (Leica VT1000S). The olfactory mucosae, the nerves and most of the brain were left intact in the preparation.

Because the connection from the olfactory epithelium to the bulb is preserved, this preparation allows us to stimulate the receptor neurons with natural odorant while performing physiological recordings in the bulb. Thus, the preparation is ideally suitable for studying the odor-evoked activity in neurons of the olfactory bulb.

2.2 Single-cell morphological reconstruction

The biocytin (0.5 %; Sigma) or Alexa Fluor 488 hydrazide (0.2 mM; Molecular Probes) was dissolved in the internal solution containing 2 mM NaCl, 11 mM KCl, 2 mM $MgSO_4$, 80 mM potassium gluconate, 10 mM HEPES, 0.2 mM EGTA, 3 mM ATP dipotassium salt, 0.1 mM GTP dipotassium salt (190 mOsm, pH 7.8; Sigma) and then filtered. The pH and osmolarity of the solution after adding the biocytin or Alexa 488 were re-adjusted to 7.8 and

190 mOsm, respectively. The solutions were stored at -20 ˚C.

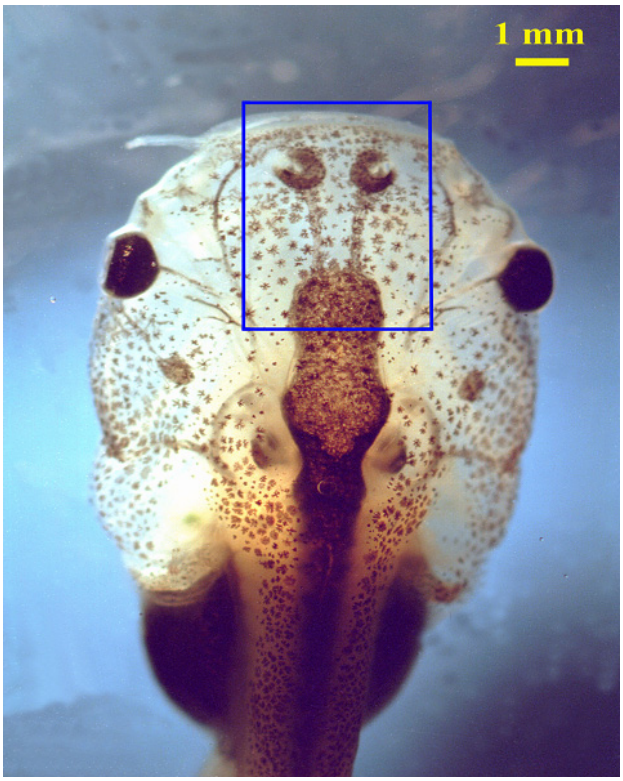

Fig. 2.1 The tadpole nose-brain preparation. The olfactory system of *Xenopus laevis* tadpoles is the focus of this study. The blue rectangle indicates the block of tissue containing most part of the olfactory system that we isolate for physiological recordings.

For juxtacellular iontophoresis, patch electrodes were fabricated from borosilicate micropipettes with 1.8 mm outer diameter (Hilgenberg) using two-stage pipette puller. The pipettes were loaded with the biocytin or Alexa 488 hydrazide solution. After the establishment of the loose seal on-cell configuration (seal resistance: 20-50 MΩ), biocytin or Alexa 488 was delivered into the cell using iontophoresis protocol consisting of short current pulses (2 ms; 1.5 to 2 nA) delivered at 1 Hz for several minutes. To avoid ambiguity, only one cell was chosen for staining in each bulb.

To develop the biocytin staining, the preparation was fixed in 4%

paraformaldehyde (Sigma) and left overnight. After rinsing several times to remove the fixative, the tissue was incubated in 0.1M phosphate buffer saline containing 5µg/ml Avidin-conjugated Alexa 488 and 0.2% Triton-X 100 (sigma) for 24 hours at 4˚C. The olfactory bulbs were then excised, isolated from the tissue block and mounted using 85 % of glycerol as mounting media. For experiments where Alexa-488 was directly injected into the cell, the tissue was fixed in paraformaldehyde (4 %) for 2 hours and then mounted for observation as previously described.

Fluorescence labeled single neurons were imaged using a confocal laser-scanning microscope (Zeiss LSM510 attached to an Axiovert 100M). A series of optical sections at different depth were imaged and stored as three-dimensional stacks. For displaying purpose, optical sections were projected into one image and then imported into Adobe Photoshop (Adobe) for further contrast enhancement.

2.3 Electrophysiological recordings

Each session of electrophysiological recording was carried out using a freshly prepared nose-olfactory bulb preparation and finished within 2 to 4 hours. The preparation was placed in a recording chamber under an upright microscope (Axioskop 2, Zeiss) equipped with a long-working distance, 40x objective (Zeiss) and differential interference contrast (DIC) optics for enhancing the contrast of living-tissue images. Throughout the recording, the preparations were superfused with frog Ringer's solution. The current and voltage were recorded using an EPC-7 patch-clamp amplifier. The signal was filtered with the built-in Bessel filter at 3 kHz, digitized at 10 kHz, and stored to disk using a custom-built acquisition hard- and software.

2.3.1 Loose-seal on-cell patch clamp recordings

The loose-seal patch clamp technique was used in this study to record AP-induced currents because we occasionally observed $[Ca^{2+}]_i$ increases when the cell membrane formed a tight seal with the glass pipette (a similar effect was described in rat somatotropes, Robert *et al.*, 1999). A low seal resistance of 20 to 50 MΩ in the on-cell loose-seal patch clamp allowed spike detection while preserving a normal $[Ca^{2+}]_i$ activity . To confirm that the patch recording did not alter the $[Ca^{2+}]_i$ activity, we recorded the $[Ca^{2+}]_i$ response of a cell of interest prior to and after the loose patch was established. The recording was discarded if the responses before and after patching differed significantly.

For on-cell loose-seal recording, we used relatively large pipettes with resistances of ~ 2-3 MΩ when filled with solution containing 98 mM NaCl, 2 mM KCl, 3 mM $MgCl_2$, 10 mM HEPES, 0.2 mM EGTA (230 mOsm, pH 7.8; Sigma). A small positive pressure (~30 hPa) was constantly applied to the pipette while approaching the cell. When a pipette tip was placed against a cell membrane, the release of the positive pressure was sufficient to let the seal resistance increase to ~20 – 50 MΩ. The current flowing through the electrode was recorded while the electrode potential was clamped at 0 mV.

2.3.1 Whole-cell patch clamp recordings

Whole-cell patch clamp recordings were performed using pipettes with smaller tip diameters. The pipette resistance was 7-11 MΩ when filled with internal solution containing 2 mM NaCl, 1 mM KCl, 2 mM $MgSO_4$, 90 mM potassium gluconate 10 mM HEPES, 0.2 mM EGTA, 3 mM ATP dipotassium

salt, 0.1 mM GTP dipotassium salt (190 mOsm, pH 7.8; Sigma). This recording solution contains a low concentration of chloride ion (1mM) and is used in all whole cell voltage-clamp and current-clamp data shown in this thesis.

To avoid a large electrode potential caused by a direct contact between silver-chloride electrodes and low Cl^- internal solution, we designed a specialized agarose bridge (Fig. 2.2). The silver-chloride electrode was inserted into a plastic tube filled with high Cl^- solution-based agarose gel. The agarose-insulated electrode was then inserted into the pipette containing low Cl^- internal solution.

In the voltage-clamp mode, several holding potentials ranging from –70 to –30 mV were used to record spontaneous postsynaptic currents (PSCs), and the holding potential of –70 mV was used to record odor-evoked PSCs. In the current-clamp mode, most cells were current-clamped at the command current of zero. However, in some cells where intracellular voltages were fluctuating in a depolarizing range with few spikes occurring, a small command current was applied in these cells to hyperpolarize the membrane potential. Voltages in all recordings were corrected for a junction potential of ~15 mV.

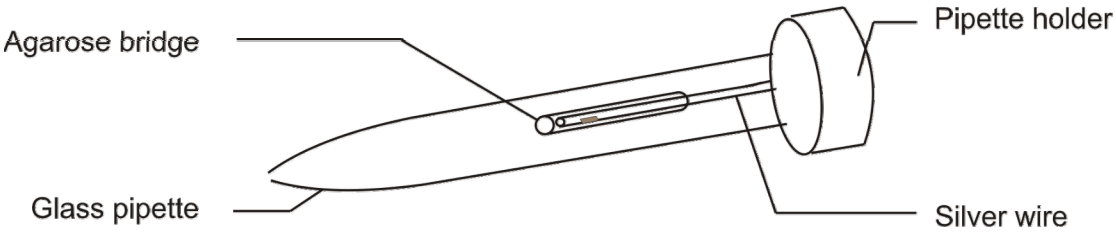

Fig. 2.2 The recording electrode with the agarose bridge. A plastic tube containing high Cl^- solution-based agarose gel was used to prevent direct contact between silver-chloride electrode and the low Cl^- internal solution.

2.4 Fura-2/AM, and the staining procedure

Fura-2 is a widely used fluorescence calcium indicator for quantitative measurements of intracellular calcium concentration ($[Ca^{2+}]_i$) (Grynkiewicz, *et al.*, 1895). Because calcium binding shifts the peak of its excitation spectrum (Fig. 2.2), ratio of fura-2 fluorescence intensities at two excitation wavelengths can be used to quantify absolute $[Ca^{2+}]_i$, independent of total dye concentration, path length, or the sensitivity of the instrument. To obtain the full dynamics of spectrum shifting in ratiometric measurements, the ratio of fluorescence intensities is often measured at excitation wavelengths of 340 and 380 nm.

The K_d value of fura-2 is around 100 nM. Thus, it is suitable for measuring $[Ca^{2+}]_i$ in the nanomolar range. However, it can be saturated at $[Ca^{2+}]$ above several μM, thus limiting its application to indicate $[Ca^{2+}]$ at a higher concentration range.

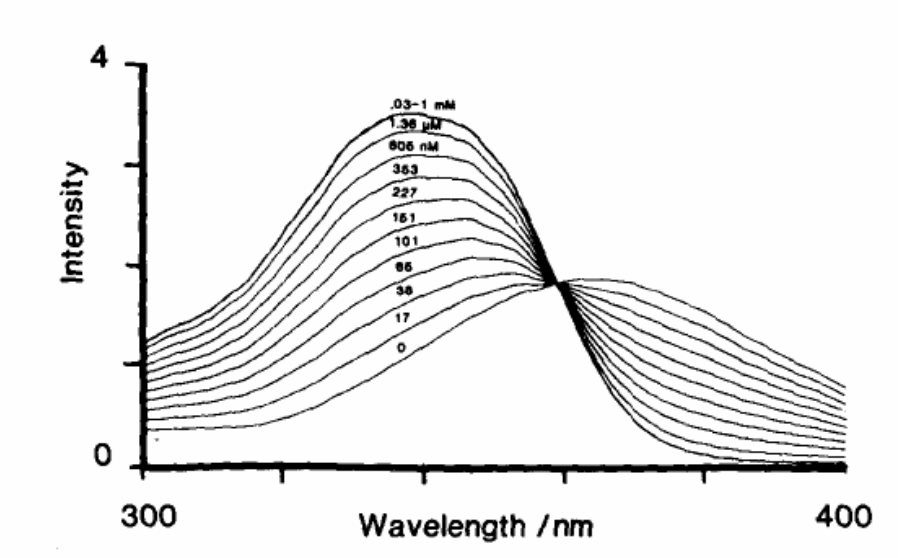

Fig. 2.3 The excitation spectrum of fura-2. The excitation spectrum of fura-2 shifts with varying [Ca^{2+}].

The acetoxymethyl (AM) ester derivative of a fluorescence indicator is uncharged and membrane permeable. Thus, it can be used to stain cells without a disruption of their membrane integrity. Once it enters the cells, endogenous esterases can cleave the AM ester group, resulting in a charged form of the indicator that can not cross the membrane. Thus, this allows the fluorescence indicator to accumulate inside the cells.

To stain neuron populations in the olfactory bulb, Fura-2/AM (Molecular Probes, Leiden, Netherlands) was dissolved in DMSO, and diluted in Ringer's solution to 50 µM. The olfactory preparation was incubated with 50 µM fura2/AM for 30 minutes at room temperature. The stained preparation was then placed under the microscope and continuously perfused with Ringer's solution. Before imaging, the preparation was washed for at least 30 minutes to remove dye in the extracellular space and to allow full de-esterification of the dye in the cytoplasm.

2.5 Calcium imaging

For calcium imaging, excitation wavelengths at 380 nm and 350nm were selected from a xenon lamp (Zeiss XBO) using a custom-built monochromator (Fig. 2.3). An optical fiber coupled the excitation light into an upright microscope (Axioskop 2, Zeiss) that was equipped with a fura-2 filter set (emission: BP 500-530, dichroic: FT 425, Zeiss). Fluorescent images were recorded using a frame-transfer, back-illuminated CCD camera (Princeton Instruments, Micromax: 512BFT) and stored on a PC using the software Winview32 (Visitron System, Munich). For experiments using single wavelength excitation, images excited at 380 nm were taken at 5 Hz with a short exposure period of 30 ms to prevent bleaching. A custom-built external shutter stopped the light between two exposures. For experiments using double wavelength excitation, pairs of images subsequently excited for 30 ms at 380 nm and 350 nm were taken at 5 Hz to cancel effects of optical path length and dye amount.

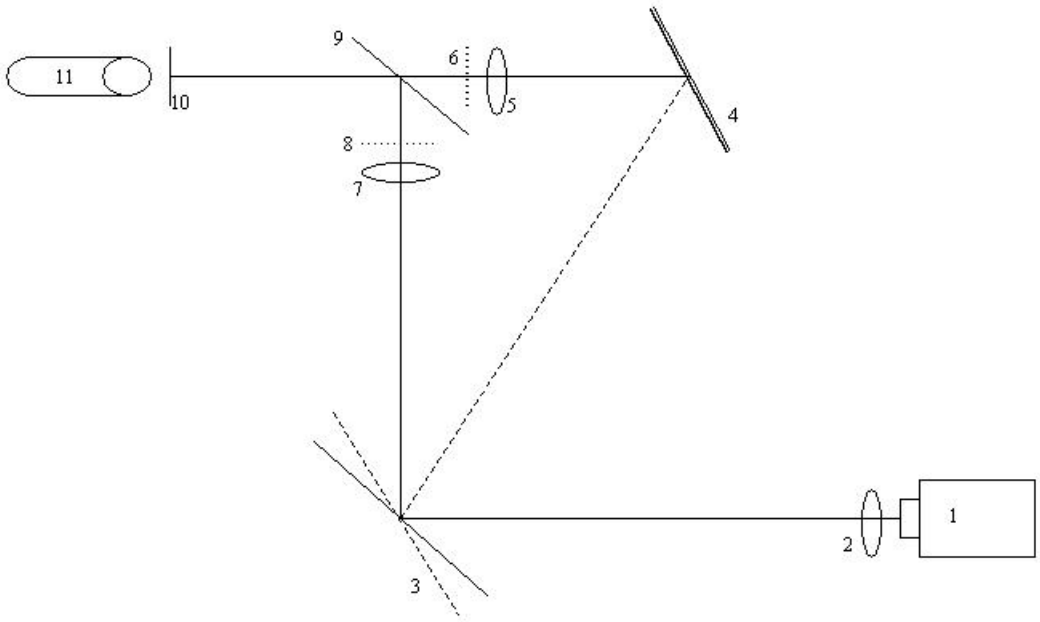

Fig. 2.4 Schematic of the monochromator. The custom-made monochromator has 11 components. The UV light coming from a xenon lamp (1) is focused by a lens (2) and reflected by a dichroic mirror (3). The dichroic mirror is mounted on a galvanometric motor, which switches between two different angles to conduct the light into two different paths indicated by the full line and the dotted line. On the full-line light path, the light of 350 nm is focused by a lens (7), filtered by a low pass filter (8) and reflected by the second dichroic beam splitter (9). On the dotted-line light path, the light of 380 nm is first reflected by a reflective mirror (4), focused by a lens (5), filtered by a band pass filter (639±10 nm), and pass through the second dichroic beam splitter (9). Both wavelengths of light are collected by the optic fiber that couples the light into the microscope (11). A shutter (10) in front of the optic fiber controls the light entering the fiber.

2.6 Calibration

To allow the conversion from Fura-2 fluorescence ratio to $[Ca^{2+}]_i$, we carried out calibration experiments by loading cells with solutions containing Fura-2 and Ca^{2+} at various defined concentrations (C_{low}, C_{def}, C_{high}; see Table 2). The calibration solutions were loaded into bulbar cells via patch pipettes, and the fluorescence intensities at both excitation wavelengths were measured using the set-up described above. The fluorescence background in calibration experiments were measured as the intensity before the cell was loaded with the dye. The ratios (F351/F382) at C_{low}, C_{def}, and C_{high} were 0.292, 0.911 and 3.565 respectively. The effective dissociation constant of fura-2 was calculated to be 1.094 μM.

(mM)	KCl	$CaCl_2$	EGTA	BAPTA	Fura-2	HEPES
C_{low}	**86**	**0**	**10**	**0**	**0.1**	**1**
C_{def}	**81**	**5**	**0**	**10**	**0.1**	**1**
C_{high}	**79**	**10**	**0**	**0**	**0.1**	**1**

Table 2 Composition of the calibration solutions. These three solutions were used in the calibration procedure to measure the effective dissociation constant (K_{eff}), R_{min}, and R_{max}. The calibration was performed by loading the dye into the cells through patch pipettes.

2.7 Odorant stimulation and a criterion for defining stimulus-specific responses

A mixture of 14 L-amino acids (alanine, serine, threonine, cysteine, valine, leucine, isoleucine, methionine, proline, arginine, lysine, histidine, phenylalanine, and trytophan, 200μM in frog Ringer's solution, Sigma, Inc.) was used as odorant stimulation to the olfactory receptor neurons. As neurons in the olfactory bulb might respond to pressure changes in the stimulus flow (Zippel and Breipohl, 1975), an odorant application device was used to keep the pressure change lower than 11 mPa while odorant solution was added through the device to the olfactory epithelium (Schild, 1985). As a control, we applied bath solution in the same way as we applied mixed amino acids to make sure that stimulus-evoked responses were due to the mixed amino acids rather than to any other sources.

Due to the ongoing activity in the OB, some peaks of the spontaneous $[Ca^{2+}]_i$ fluctuation could easily be mistaken for stimulus-induced responses. We therefore established a protocol that consisted of the recording of ongoing $[Ca^{2+}]_i$ activity for one minute, followed by three identical stimulus applications, one each minute. The response was assumed if the repeated stimulus responses were similar with each other with the averaged correlation coefficient above 0.4. The three response fluorescence waveforms were then averaged to extract a stimulus-specific component.

2.8 Calcium imaging combined with patch recording

For simultaneous recording of $[Ca^{2+}]_i$ and action potentials, we combined fura-2 imaging with the on-cell loose-seal patch clamp technique. In this type of experiments, the neuron populations were first loaded with fura-2-AM. Calcium imaging was then performed using the full size of the CCD chip to record many cells in a field of view. Every image sequence was analyzed

immediately and a cell showing either spontaneous $[Ca^{2+}]_i$ fluctuations or odor-evoked $[Ca^{2+}]_i$ responses was selected and re-identified in the transmission mode. After the on-cell configuration was established on the chosen cell, simultaneous electrical and $[Ca^{2+}]_i$ recording was then carried out. Image acquisition was triggered by the patch-clamp software for synchronizing the patch-clamp recording and CCD image acquisition. The trigger times were written to the patch-clamp data file to facilitate data alignment. In fast CCD imaging, $[Ca^{2+}]_i$ were sampled at 125 Hz by binning all pixels of the recorded cell into one.

2.9 Data analysis

Image analysis was carried out using Matlab (MathWorks). The fluorescence intensity time course F(t) was calculated by averaging the pixels corresponding to a soma. Because the intensity of fura-2 decreases as $[Ca^{2+}]_i$ increases when exciting at 380 nm, fluorescence traces were represented as the normalized relative fluorescence $F_n = (F_{max} - F(t))/F_{max}$, F_{max} being the maximum of F(t).

To quantify the level of spontaneous $[Ca^{2+}]_i$ fluctuations, we calculated the proportion of the increasing periods to the total recording time, and named this proportion the “mean activity index” (MAI). In order to distinguish a significant increase in fluorescence from an increase caused by noise, we applied the paired t-test to the intensities of a cell’s individual pixels at t and at t + dt. The time point t is included as part of the rising phase if the test is significant at a level $p<0.001$.

In order to determine the points in time when AP-related currents occurred in the recorded current traces, the cross-correlation function

between an AP-associated current template and the whole current trace was calculated. Peaks of this function indicated the occurrence of an action potential.

3. Results

3.1 Laminar organization and cell morphology of Xenopus laevis tadpole olfactory bulb

As in other vertebrates, the tadpole olfactory bulb is organized in layers containing nerve ending layers (e.g. the layer of glomeruli; the implantation cone) or cell body layers (e.g. the mitral and granule cell layer) (Scalia *et al.*, 1991; Nezlin & Schild, 2000). The layered structure can be seen in fluorescence images where cell bodies are brightly stained (Fig. 3.1B). From the fluorescence image, two cell layers can be clearly visualized as a cell-poor gap separating the rostral layer from the subjacent caudal layer next to the ventricle. According to previous morphological studies, these two layers of cells correspond to the mitral and granule cell layers, respectively (Czesnik *et al.*, 2001; Czesnik *et al.*, 2003).

The identity of the cells in these two layers was further confirmed using single-cell morphological reconstruction. This was done either by allowing tracers to diffuse into the cell during whole-cell recording, or by tracer iontophoresis during on-cell extracellular recording (see methods and Pinault, 1996). As long as the morphological information is the only purpose of the experiment, the latter technique is considerably faster and easier because it does not require the formation of giga-seal (usually a seal resistance in 20-50 MΩ is sufficient), and it makes the detachment of pipettes from the cell much easier. In this preparation, several minutes of extracellular iontophoresis is usually sufficient to give a bright staining when either biocytin or Alexa-488 was used as tracer molecules.

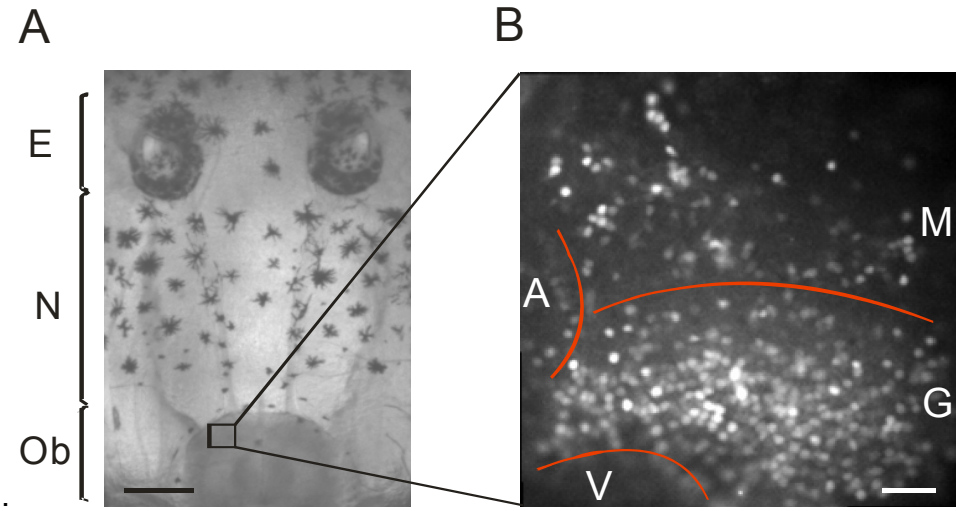

Figure 3.1 Layered structure of the *Xenopus laevis* tadpole olfactory bulb. (A) The nose-brain preparation contains the olfactory epithelia, olfactory nerves, and olfactory bulbs from tadpoles of *Xenopus laevis*. E, olfactory epithelium; N, olfactory nerve; OB, olfactory bulb. Scale bar, 0.6 mm. (B) Fluorescence image of a fura-2/AM-loaded olfactory bulb taken at 380 nm excitation. Cell layering in tadpole's olfactory bulbs is clearly visible. M, mitral cell layer; G, granule cell layer; A, accessory bulb; V, ventricle. Scale bar, 32 µm.

Fig 3.2 to Fig 3.4 shows the single cell morphology of typical cells whose soma resides in the rostral cell layer. The morphology of these cells contained features that (i) thin axons extended caudally, (ii) thick primary dendrites went rostrally toward the glomerular layer, (iii) primary dendrites highly branched at their terminals, a structure termed "tufts" (Fig. 3.2 -3.4). These features closely matched the mitral cell (MC) morphology described previously (Shipley & Ennis, 1996), indicating the MC identity of the cell sampled from the rostral mitral cell layer. Consistent with previous descriptions of MC morphology in amphibians (Scalia *et al.*, 1991), we observed that the axon of these cells could arise either from their cell bodies (Fig. 3.2) or from dendrites (Fig. 3.3). Moreover, in sharp contrast to mammals, where each MC typically innervate only one glomerulus, MCs in tadpoles and other amphibians can send their

dendrites into one or more than one glomeruli (Fig. 3.4 and Jiang & Holley 1992). The multiple-glomerular MCs are also known to be present in fish, in some insects and in mammalian accessory bulb (Satou, 1990; Fujita *et al.*, 1988; Takami & Graziadei, 1990, 1991), and could represent different odor processing strategy emerged throughout the course of evolution.

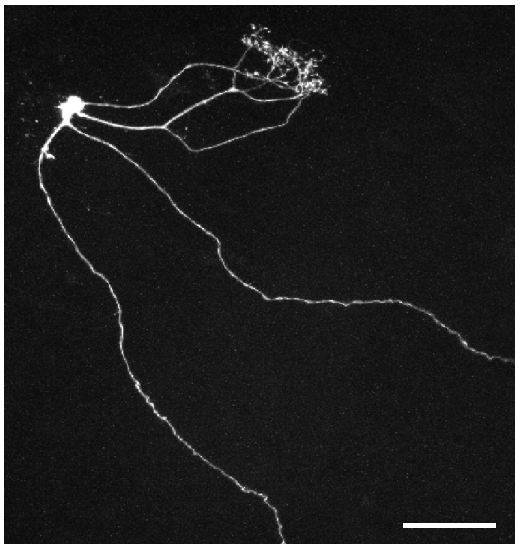

Figure 3.2 Morphological reconstruction of a single neuron in the mitral cell layer. The cell shows two primary dendrites that branch several times before entering the same glomerulus. Two thin axon-like processes extend caudally from the soma. Scale bar: 50µm.

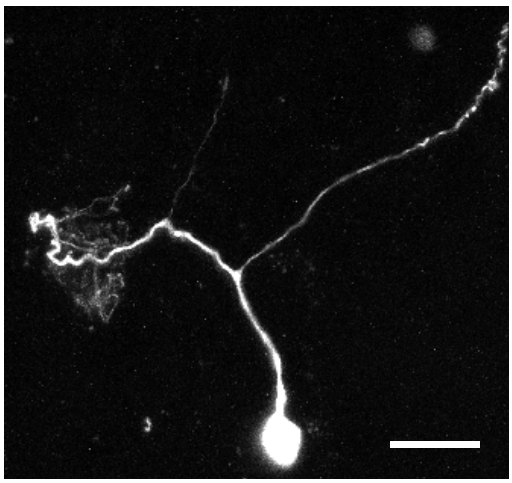

Figure 3.3 Morphological reconstruction of a single neuron in the mitral cell layer. The cell shows single primary dendrites that innervate one glomerulus. The axon of this cell arises from its primary dendrite. Scale bar: 20μm.

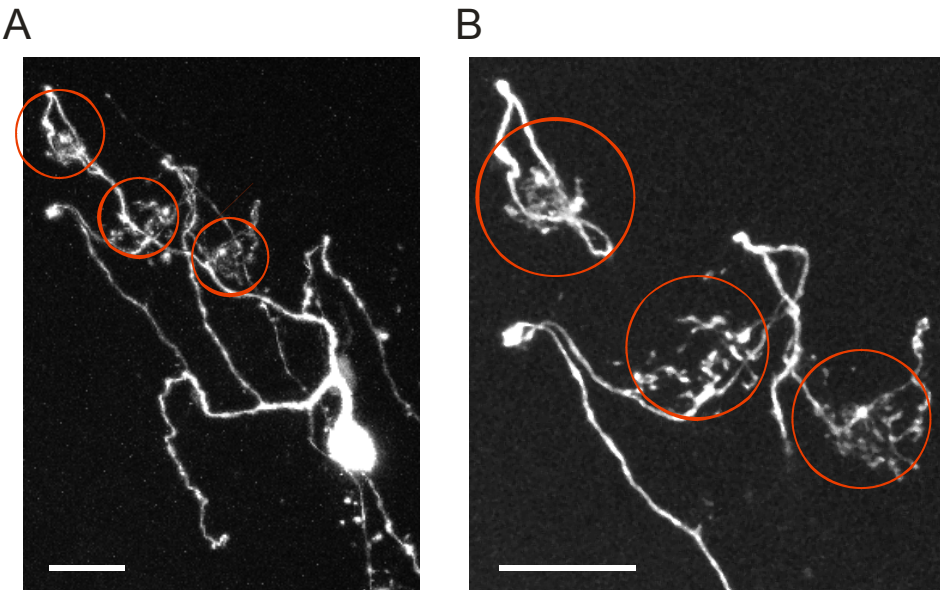

Figure 3.4 The Multiple-glomerular mitral cell. The dendrites of this mitral cell branch extensively in the glomerular layer and show three distinct glomerular tufts (red circle). Scale bars: (A), (B) 20μm.

In contrast to cells in the mitral cell layer, the cells sampled from the granule cell layer extended their dendrites rostrally into the mitral cell layer and showed no processes projecting out of the olfactory bulb. The most prominent morphological feature of olfactory bulb granule cells (GCs) is their dendritic spines, i.e. the tiny protrusions from the dendrites (Fig. 3.5). The dendritic spine in GC has been suggested to be the site of dendrodendritic inhibition between MC and GCs. (Shepherd, 1972)

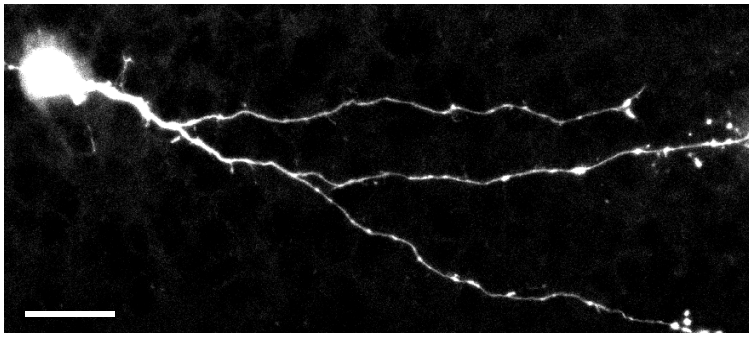

Figure 3.5 Morphological reconstruction of a single neuron in the granule cell layer. The cell has several thick spiny dendrites extending rostrally into the mitral cell layers. Scale bar: 10μm.

Unexpectedly, we observed in one case where dye injection into a single cell in the mitral cell layer unambiguously labeled another cell in the same layer as well as a cell in the granule cell layer (Fig. 3.6). Such staining is unlikely to be due to nonspecific tracer uptake from extracellular space because we could clearly identify the connection between the injected cells and the two other labeled ones (Fig. 3.6B). Interestingly, although two of the stained cells were located in the mitral cell layer and their dendrites branch extensively, both of them did not possess glomerulus tufts, suggesting they may correspond to developing MCs. Gap junctions may couple neurons during the formation of neuronal circuitry (Naus & Bani-Yaghaub, 1998; Montoro & Yuste, 2004). Whether they contribute to the development of olfactory system is an interesting question and could further be tested by performing similar experiments in different developmental stages.

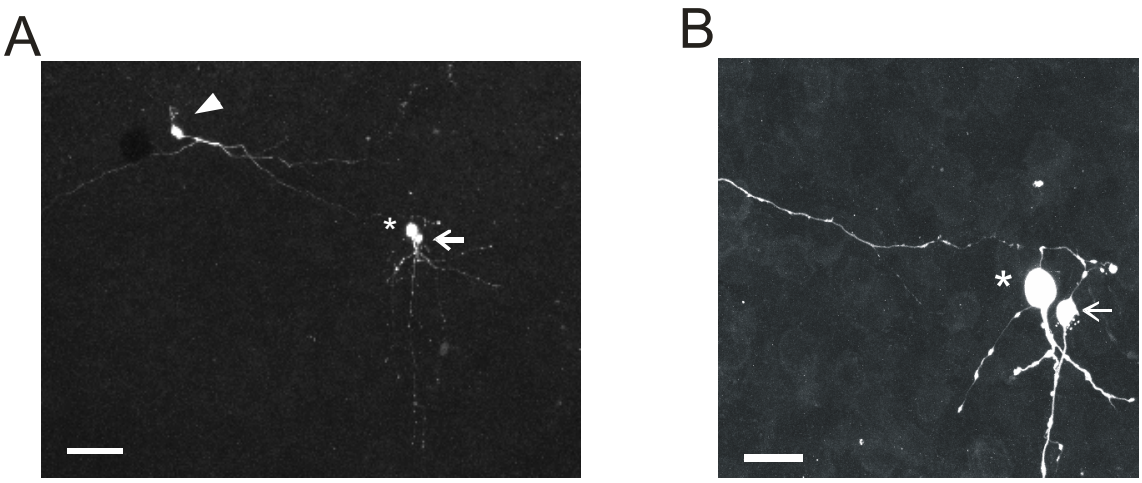

Figure 3.6 Dye coupling in the olfactory bulb (A) Dye injection into a single cell in the mitral cell layer (arrow) labeled a nearby cell (asterisk) and a distant cell in the granule cell layer (arrow head) (B) The connections between the labeled cells are clearly visible. Scale bars: 40μm for A, 20μm for B.

3.2 Electrical activities in olfactory neurons

3.2.1 Spontaneous electrical activities in olfactory receptor neurons, mitral cells and granule cells

Knowing the morphological features of the neurons in the olfactory bulb, we next investigated their electrophysiological properties. The on-cell loose-seal patch clamp was used to record action potentials on the soma. In the absence of stimulation, both MCs and GCs can generate action potentials spontaneously, which can be detected as downward deflections of the capacitive current in the on-cell recording traces (Fig 3.7). The spontaneous firing rate in MCs (1.44 ± 0.35 Hz, n = 12) and in GCs (0.91 ± 0.15 Hz, n = 15)

were similar. However, the mean firing rates of both types of olfactory bulb neurons were significantly lower than the spontaneous firing rate of olfactory receptor neurons (2.75 ± 0.63 Hz; n = 10).

In addition to the firing rate, several other differences in the spontaneous spiking pattern were observed in the three types of olfactory neurons. First, whereas the amplitude of action potential-induced on-cell current remains roughly constant for subsequent spikes in olfactory receptor neurons, current amplitudes can vary significantly from spike to spike in the same MC or GC (Fig. 3.7, 3.8). Second, the majority of MCs fire action potentials in bursts. Within a single burst, the current amplitudes often decrease progressively (Fig. 3.7B, 3.8 and 3.9). In contrast to the bursting pattern observed in MC, the firing pattern of most GCs appeared to be random (Poisson-like) (Fig. 3.7 C).

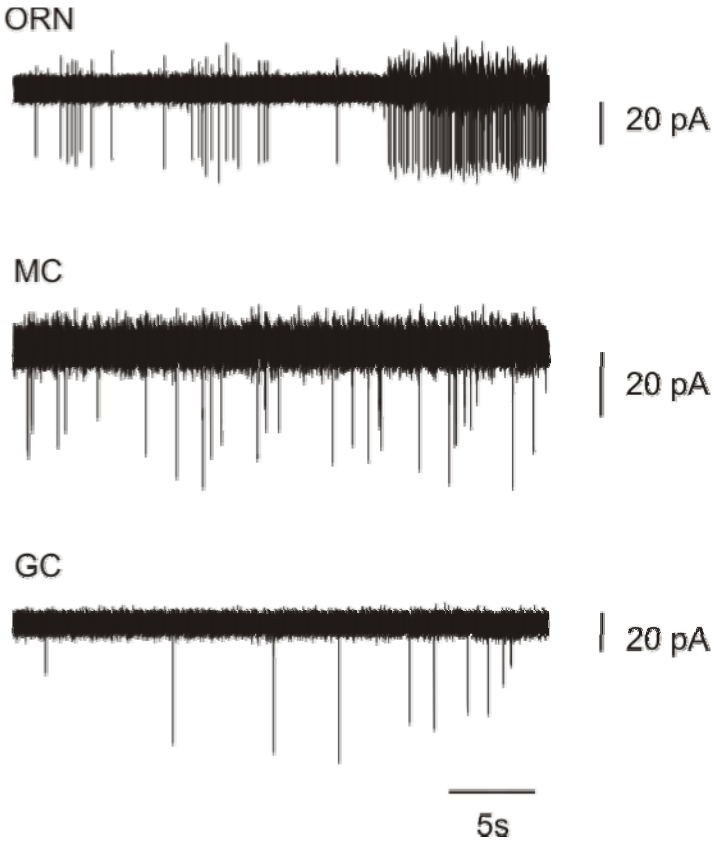

Figure 3.7 Spontaneous activity of olfactory neurons Action potential-induced capacitive currents in (A) olfactory receptor neurons, (B) mitral cells and (C) granule cells were recorded in the on-cell configuration. Whereas the amplitudes of all spikes are similar in one olfactory receptor neuron, they can vary from spike to spike in a mitral or granule cell.

The bursting behavior of MCs is also evident when analyzing the histogram of their inter-spike intervals. The inter-spike interval histogram of a bursting cell (exemplified in Fig. 3.8B) clearly showed a peak at 40 ms, corresponding to the intra-burst spiking interval and an additional component in longer interval range, corresponding to the various inter-burst intervals (Fig. 3.8B). The decay phase of the histogram can not be fitted by an exponential curve indicating that the occurrence of spike events in MC is not a Poisson point process.

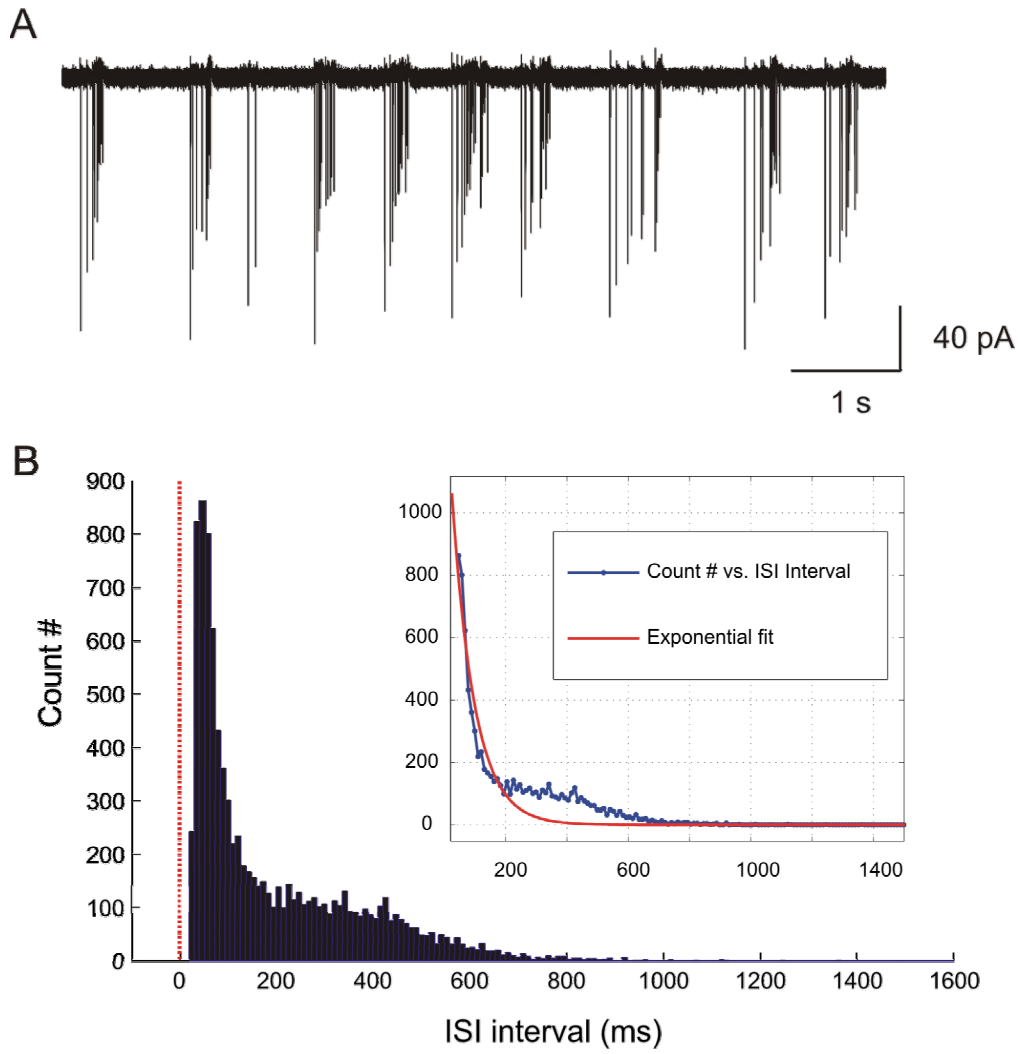

Figure 3.8 A typical mitral cell showing bursting activity (A) The spontaneous firing pattern of a typical bursting mitral cell. (B) The inter-spike interval (ISI) histogram of the same mitral cell shows a peak at 40ms, corresponding to intra-burst ISI and a tail in longer interval range, corresponding to various inter-burst intervals. Inset, the ISI histogram can not be fitted by a single exponential function.

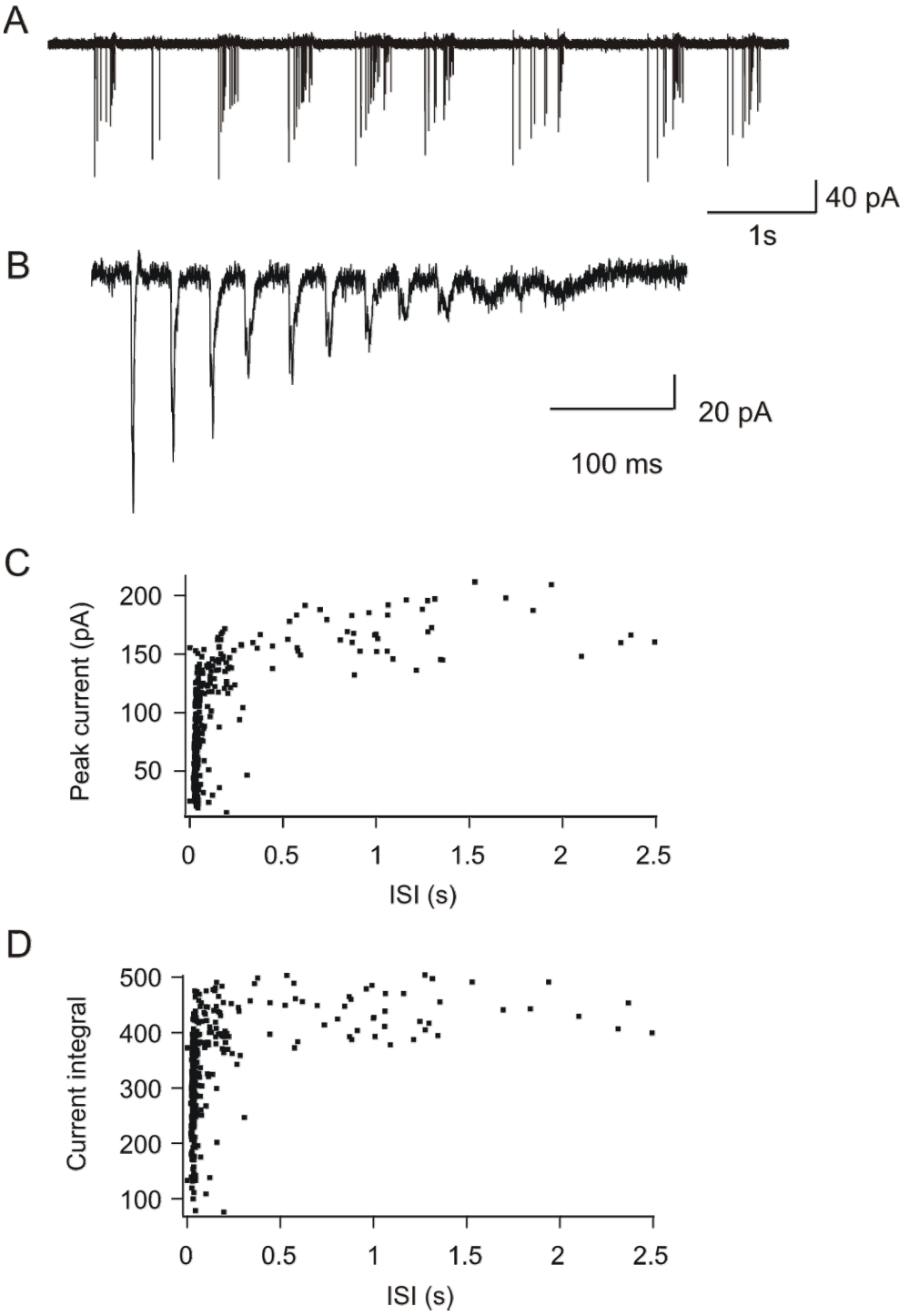

Figure 3.9 AP-induced current amplitudes in a bursting cell decrease within a burst. (A) The spontaneous firing pattern of a bursting MC. (B) AP-induced current amplitude decrease progressively within a burst. Peak amplitudes (C) and the integral (D) of AP induced capacitive currents are plotted against inter-spike interval (ISI). The decreases in both amplitudes and integrals are evident when the ISI is smaller than ~100 ms.

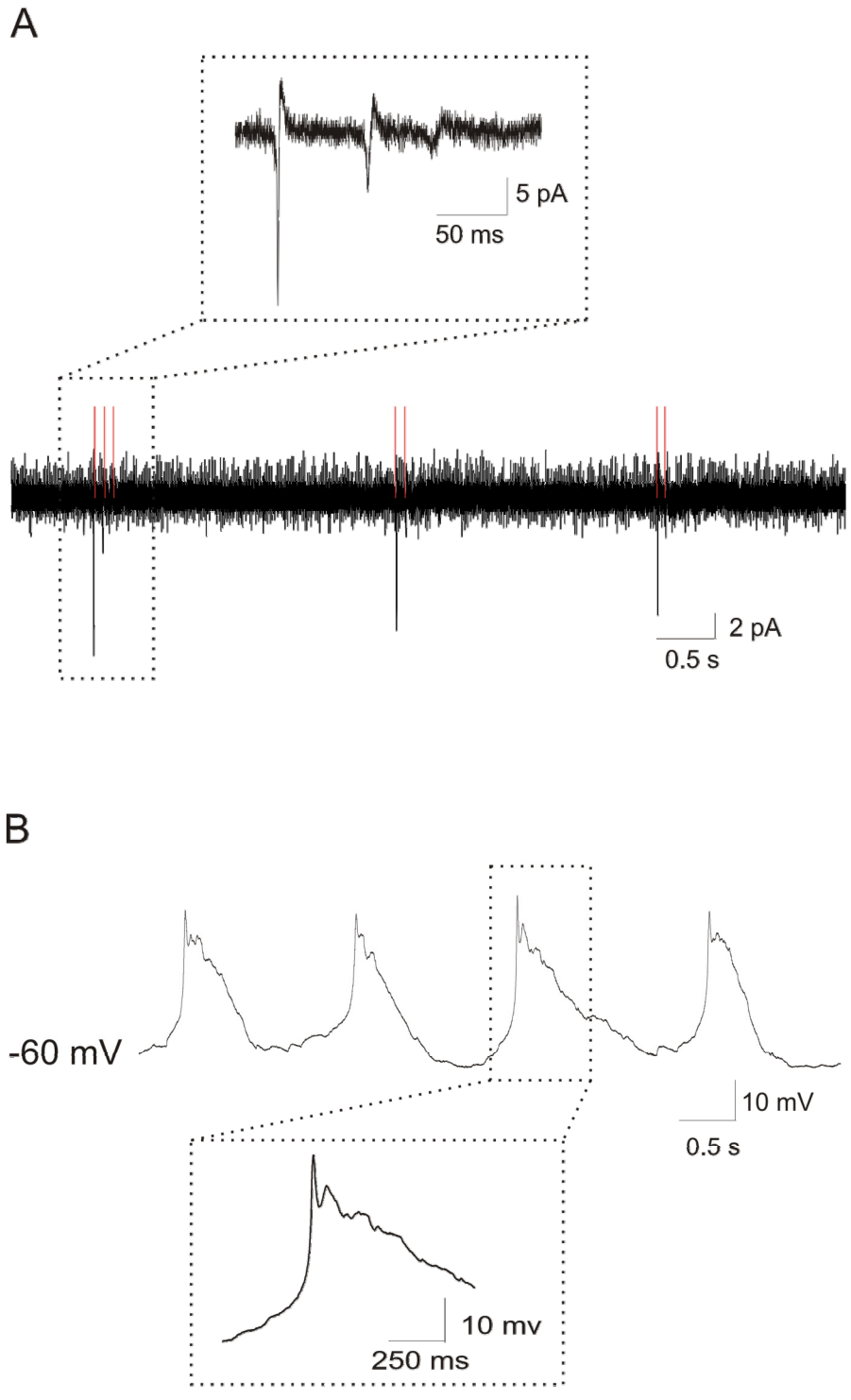

Fig. 3.10 The extracellular and intracellular recordings of spontaneous bursts in MCs. (A) MCs show the ongoing bursting behavior, and extracellularly recorded spike-induced currents are diminished dramatically within a burst. (B) In whole-cell current-clamp recordings, these MCs show large subthreshold membrane potential fluctuations, and bursting spikes are

superimposed on the top of the membrane potential fluctuations. Within one burst, the first spike has sharper depolarization voltage change and the larger peak amplitude than the second and latter spikes.

In addition to these typical spiking patterns, we also encountered a few cells in the mitral cell layer that show different characteristics of the spontaneous spiking pattern and therefore form another class. Although these cells also fire spontaneous action potentials in bursts, the number of action potentials within a single burst is much larger and the duration of the burst is far longer than the previously described bursting cells (Fig. 3.11). We thus name these cells ‘long bursting cells’ to distinguish them from the ‘short bursting cells’ that we typically encountered. Another prominent difference between these two groups of cells is that the amplitudes of action potential-induced currents in the long bursting cells (Fig. 3.11 inset) do not decrease within a burst as much as they do in the short bursting cell (Fig. 3.8 and 3.9)

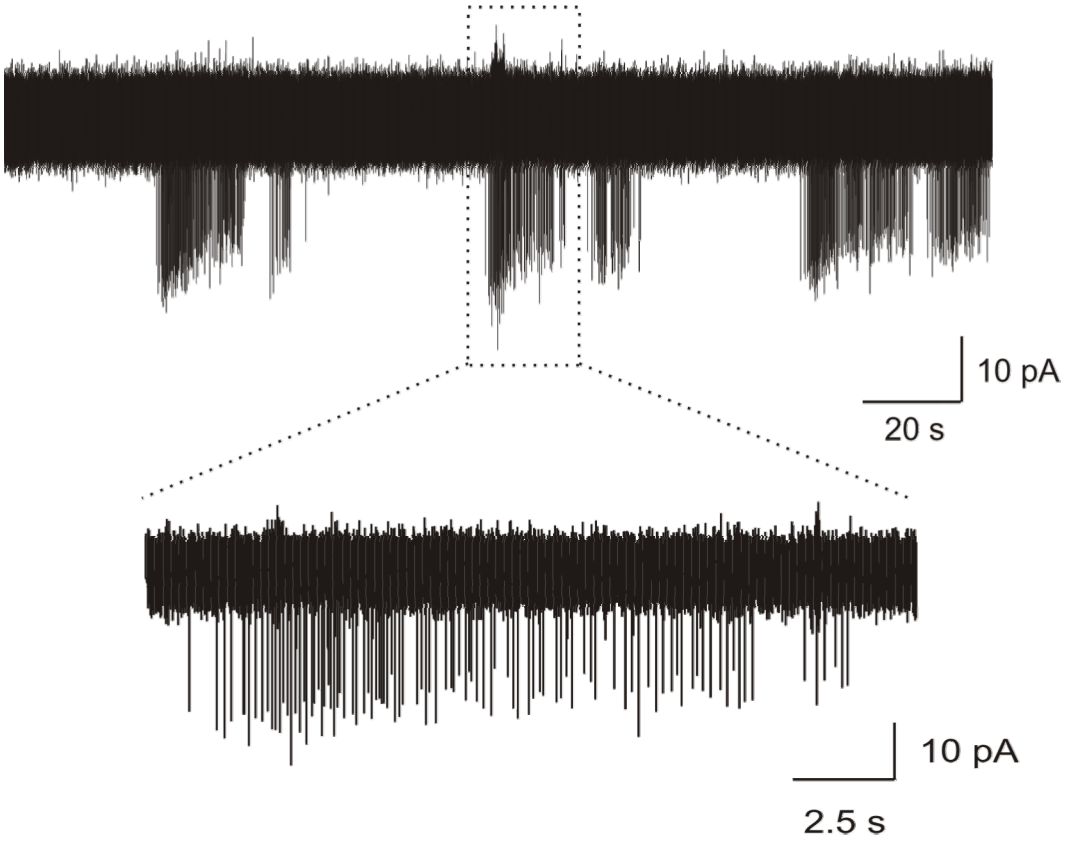

Figure 3.11 Spontaneous firing pattern of a 'long bursting cell' in the mitral cell layer. These cells show spontaneous bursting with a much longer duration than the 'short bursting cells'. Inset, the amplitudes of AP-induced currents do not decrease as markedly as in short bursting cells (e.g., Fig. 3.8).

3.2.2 Spontaneous synaptic events in olfactory bulb neurons

To investigate the characteristics of synaptic inputs of MCs and GCs, we used the whole-cell voltage clamp technique to record the spontaneous postsynaptic current in both cell types. In order to discriminate between excitatory postsynaptic currents (EPSCs) and inhibitory postsynaptic currents (IPSCs) in a single record, we used a low-chloride internal solution (see Methods) for keeping the [Cl^-] reversal potential much more negative than the

reversal potential of non-selective cation conductances. This results in a difference in EPSC and IPSC directions when membrane potential was held between these two reversal potentials, allowing us to discriminate between the two PSCs without pharmacological perturbation of the preparation.

Consistent with the widely accepted notion that MCs receive both excitatory and inhibitory inputs, we observed both inward and outward postsynaptic currents when the membrane was clamped between the two reversal potentials (n = 14; Fig. 3.12A). This result indicates that tadpole MCs already form functional synaptic connections with bulbar inhibitory networks at this developmental stage. When CNQX (100 μM) was present in the bath solution, the inward postsynaptic current was blocked while the outward postsynaptic current could still be detected (Fig. 3.12B). Thus, the spontaneous EPSC in MCs is mainly mediated by AMPA-sensitive glutamate receptors.

3.2.3 Stimulus-evoked spiking activity

To investigate how odorant stimulation modulates the electrical activities, we recorded from single bulbar neurons while stimulating the olfactory mucosae with natural odorants. The patch clamp technique was used either in on-cell configuration to record action potentials extracellularly or in whole-cell configuration to record intracellular membrane potential and synaptic events underlying the responses.

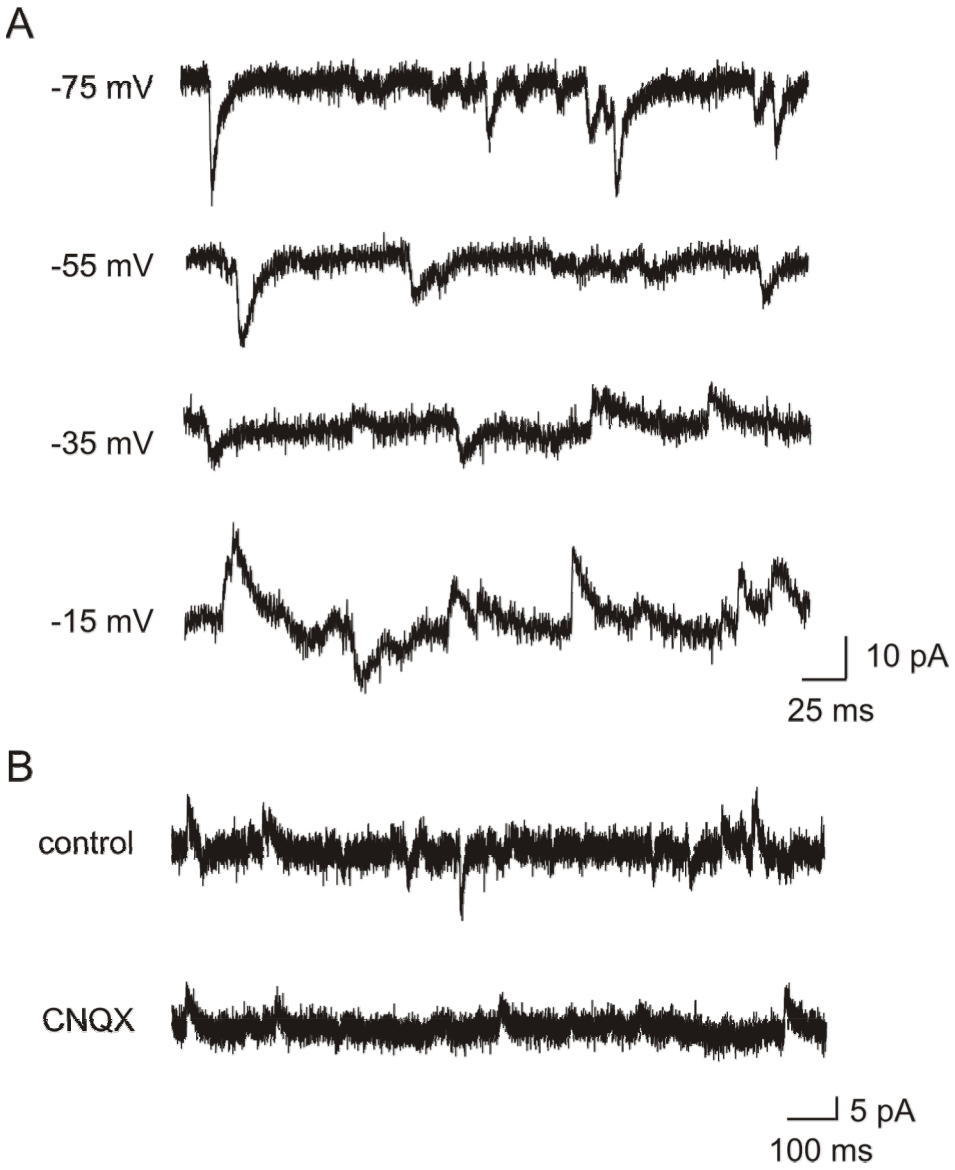

Figure 3.12 Spontaneous synaptic currents of mitral cells. (A) Spontaneous EPSCs and IPSCs at different membrane potentials. Outward IPSCs grow in amplitude when the membrane potential becomes more depolarized. (B) Most inward EPSPs were blocked by bath application of 100μM CNQX.

Odorants affected the spontaneous spiking activity of MCs either as an excitatory or inhibitory modulation. In some cells, odorant stimulation could elicit a train of spikes (Fig. 3.13A). The number of spikes evoked by odors can be substantial and the instantaneous spiking rate could be dramatically increased. In other cells, the spontaneous spiking was clearly suppressed by odorant stimulation (Fig. 3.13B). Interestingly, the onset of inhibitory responses appears to occur later than the onset of excitatory responses suggesting that the observed inhibitory response may be due to feedback inhibition from granule cells rather than a decrease in receptor neuron firing rate.

In contrast to MCs, most GCs generated only a few spikes during odorant stimulation (Fig. 3.14). Although these spikes robustly appear at certain stimulus-triggered timing over many trials, the number of odor-evoked spikes is small and the spontaneous spiking rate is only slightly increased (Fig. 3.14). On average, the number of odor-induced spikes in responding GCs is much smaller than that in the excitatory responsive MCs (5 ± 1.7 spikes in GCs (n = 11) and 16 ± 5.6 spikes in MCs (n = 6)). Thus, the number of spikes used by granule cell to code odorant information seems to be quite sparse.

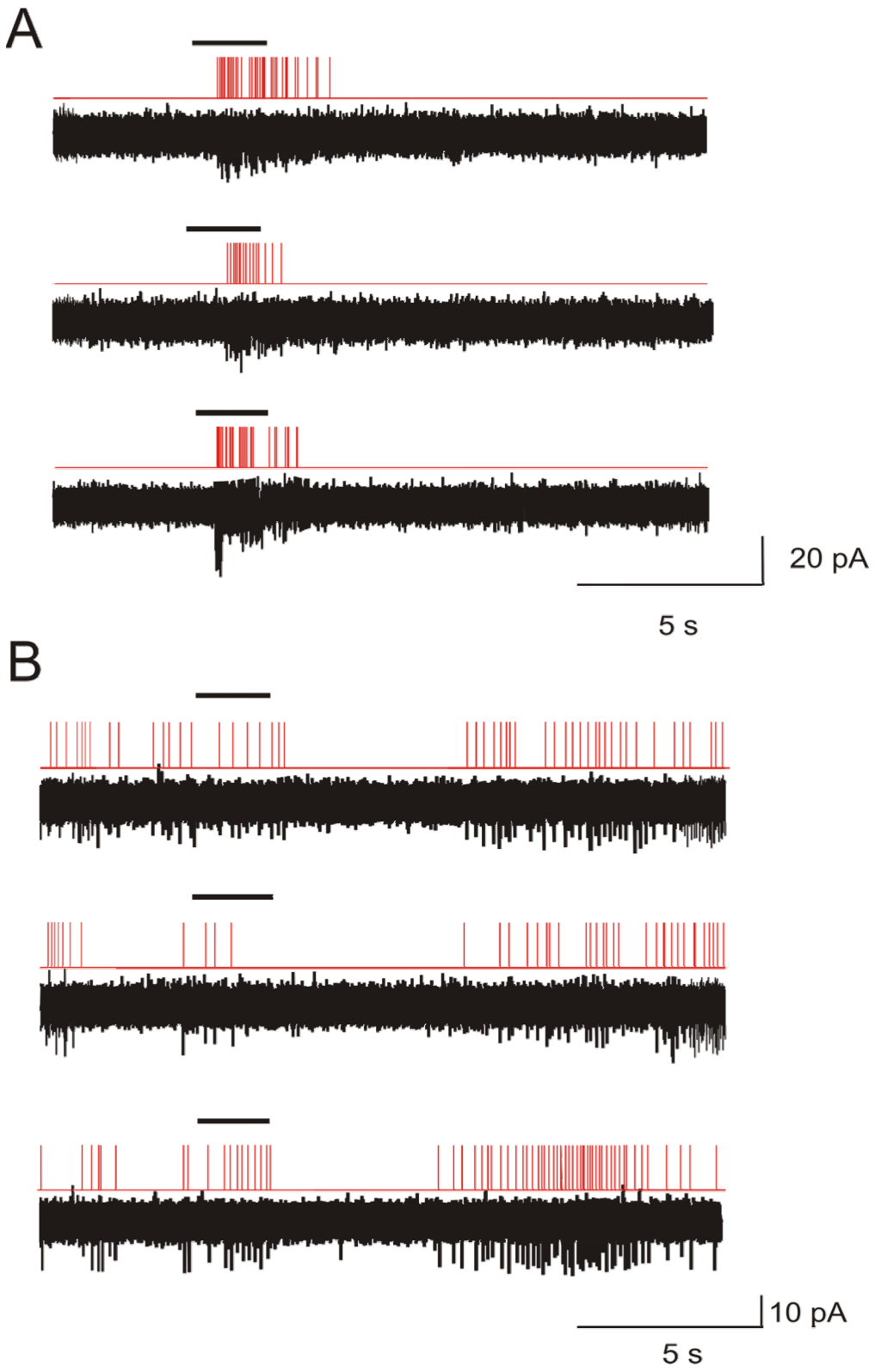

Figure 3.13 Odorant modulation of spiking activities in mitral cells. (A) A mitral cell showing excitatory response to odorant (a mixture of amino acids, see Methods). The

response pattern is highly reproducible over trials. Odorant application is indicated by a bar above the traces. (B) Another mitral cell was inhibited by the same odorant.

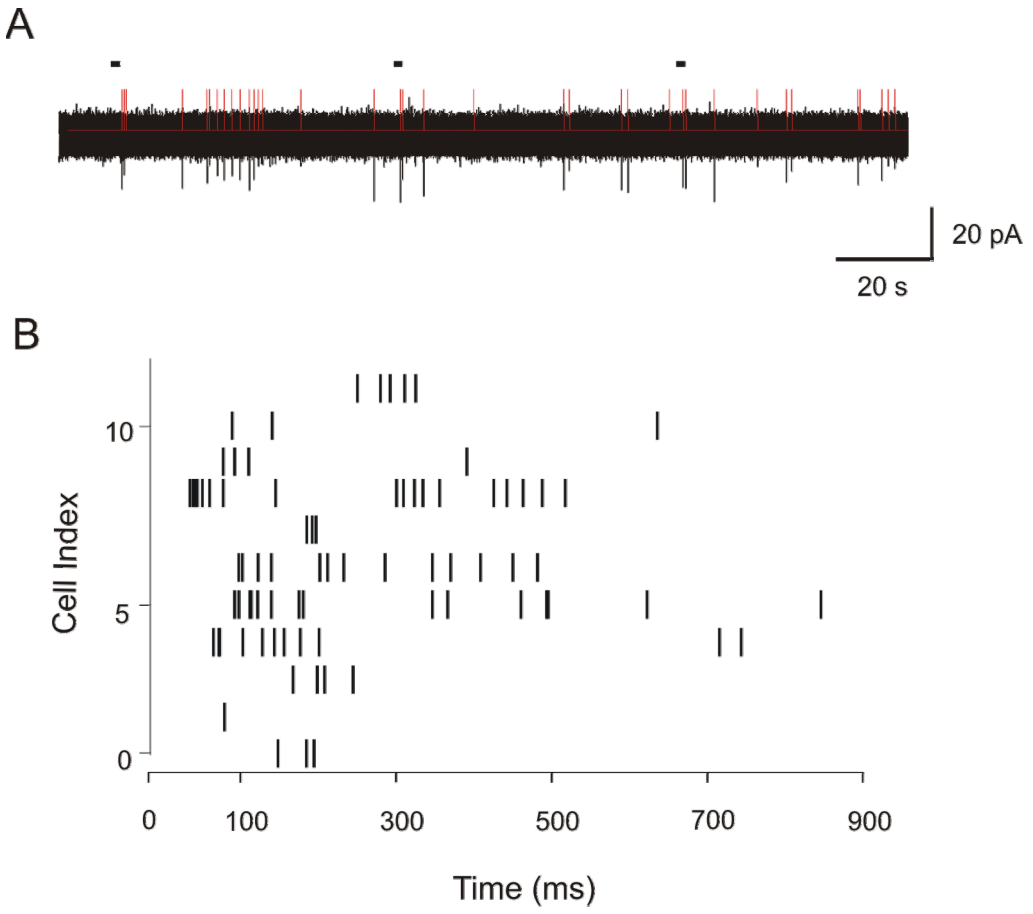

Figure 3.14 Odorant induced spiking in granule cells. (A) A granule cell showing excitatory odorant response. Upon odorant stimulation, the cell fires ~2-3 spikes. Although the odorant induced spiking is reliably observed in each trial, the firing rate of the cell is not significantly increased compared to its spontaneous firing rate. (B) Raster plot of odorant induced spiking in 11 granule cells. Each action potential is indicated by a vertical line. Odorant was applied at t=0.

3.2.4 Odor modulation of membrane potential and synaptic events

To investigate the subthreshold and synaptic events underlying stimulus evoked spiking patterns in MCs and GCs, we further used whole-cell patch clamp to record intracellular odor-induced electrical activities. In MCs showing odor-induced excitatory responses, we observed that the odorant-induced action potentials were superimposed on a small long lasting membrane potential depolarization (Fig. 3.15A). A slow inward current underlying this stimulus-evoked depolarization was clearly visible when the same cell was voltage clamped at -70mV (Fig. 3.15B). This slow inward current had similar onset timing and similar duration as the subthreshold depolarization observed in current-clamp mode. The fast EPSCs were observed both before and during stimulation and did not seem to be dramatically modulated by the stimulus (Fig. 3.15B, inset).

Consistent with previous on-cell results that there are MCs whose firing was suppressed by odor stimulation, we observed some MCs showing clear odor-induced hyperpolarization that are reproducible over trials (Fig. 3.16). Before stimulation, the membrane potential of this cell fluctuated spontaneously between - 45 mV and -55 mV with occasional fast overshoot to –35 mV, possibly due to action potentials occurring at a distal axon. In the voltage-clamp mode, a slow outward current was observed and can be associated with odorant stimuli. Despite the odor-evoked slow outward current, there were still fast EPSCs superimposed on this outward component (Fig. 3.16B).

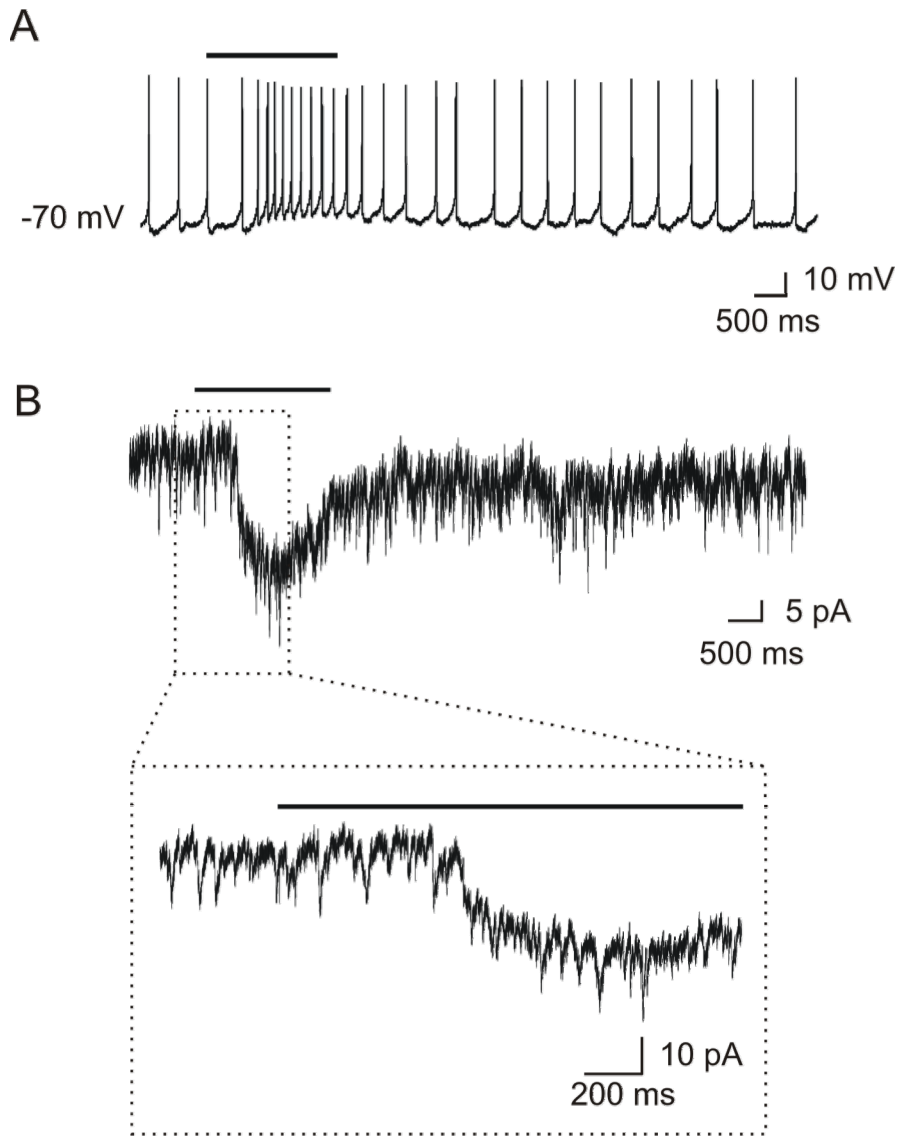

Figure 3.15 Intracellular recording of odorant induced spiking and synaptic events in mitral cells. (A) A mitral cell showing an excitatory odorant response was recorded in the current clamp mode. The odorant induced spikes were superimposed on a slow (~3s) odorant induced depolarization. (B) Voltage clamp recording of the same cell reveals an odorant induced inward current with similar duration as the slow depolarization in (A). Inset, fast EPSCs were observed both before and during odorant responses.

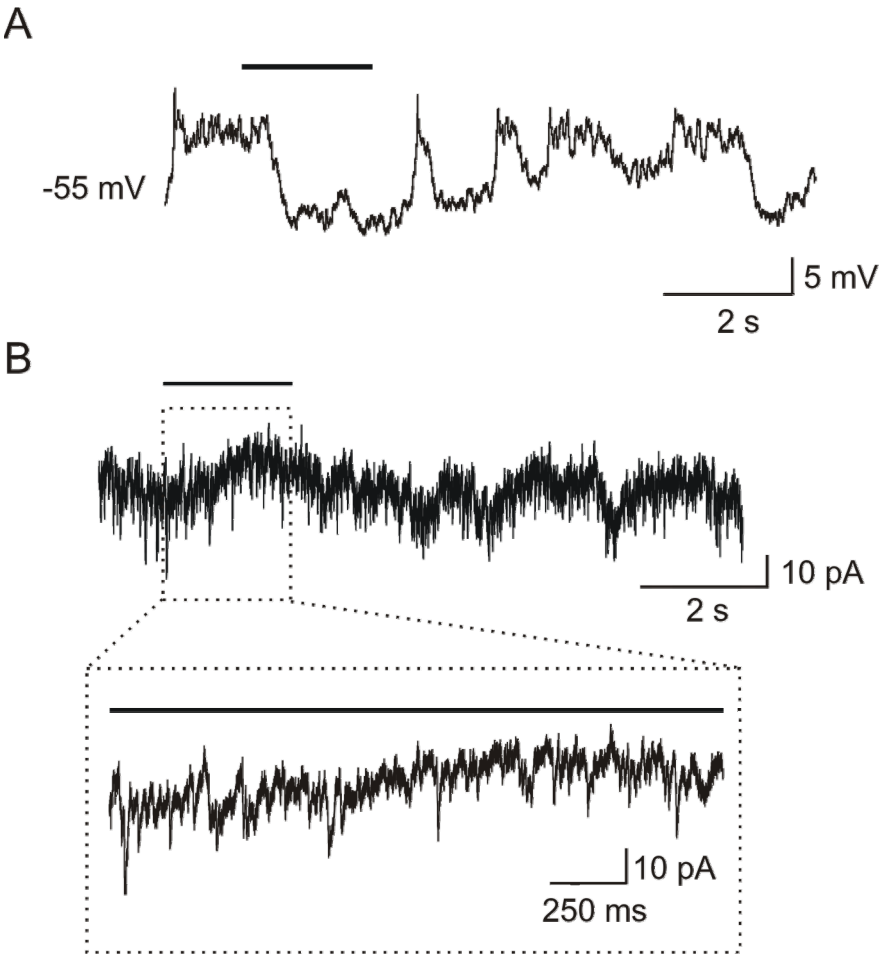

Figure 3.16 Intracellular recording of odorant induced hyperpolorization and synaptic events in mitral cells. (A) The membrane potential of this mitral cell showed a clear odorant induced hyperpolarization. (B) Voltage-clamp recording of the same cell reveals an odor induced slow outward current. Inset, fast EPSCs were observed both before and during odorant induced slow outward current.

Whole-cell patch clamp was also used to investigate intracellular odor-evoked responses in GCs. In some cells, we observed that odorant could elicit a subthreshold depolarization with only one or a few action potentials superimposed on the depolarization (Fig. 3.17A). The small number of stimulus-induced spikes is consistent with the observation in on-cell recording (Fig. 3.14A). When voltage-clamping the cell at -70mV, we observed that the odorant stimulation induced a barrage of fast EPSCs (Fig. 3.17B) rather than a long lasting inward current observed in the excited MCs (Fig. 3.15B), suggesting a different synaptic mechanism underlying the stimulus responses in GCs.

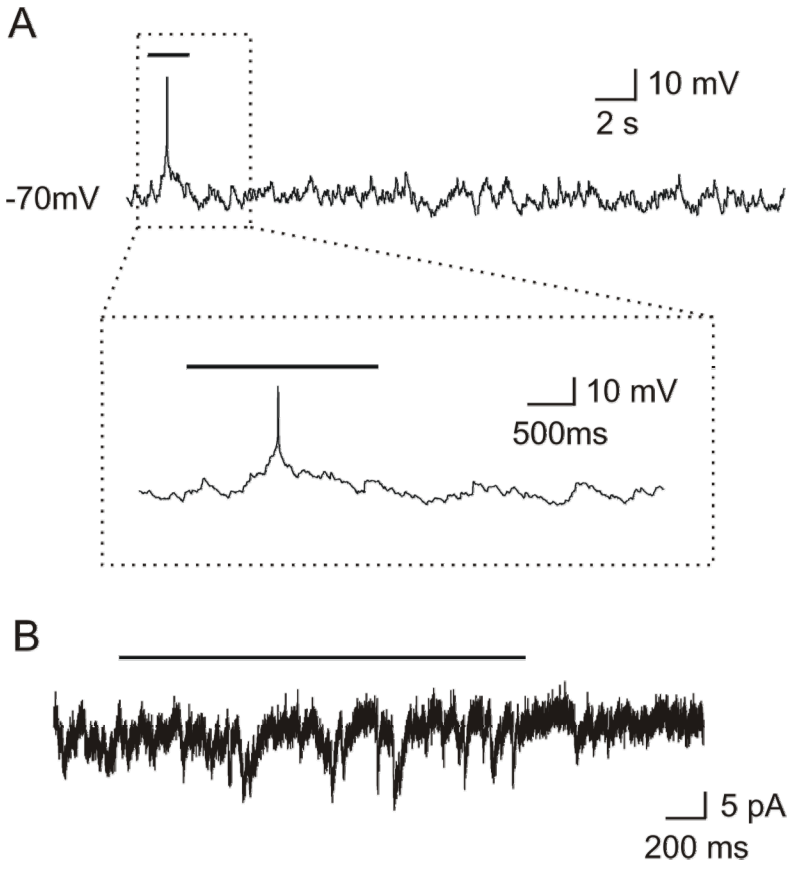

Figure 3.17 Intracellular recording of odorant induced spiking and synaptic events in granule cells. (A) Odorant stimulation induced a brief depolarization and a single action

potential in this granule cell. (B) Voltage-clamp recording of the same cell reveals a barrage of fast EPSCs during odorant stimulation.

In the whole-cell recording of a particular granule cell, we observed that the odorant stimulation elicited a long-lasting subthreshold depolarization superimposed by a few large spikes and many smaller “spikelets” (Fig. 3.18A). Both the large and the small spikes (asterisks, inset Fig. 3.18A) can be clearly distinguished from the EPSPs (arrow, inset Fig. 3.18A) by their much larger and faster depolarization. The amplitude of the large spike was about 40 mV starting from the foot whereas the smaller spikelets showed an amplitude of only about 10 mV. Moreover, the depolarizing phase of the large spike showed three distinct steps of voltage integration (Fig. 3.18B, left), whereas the ‘spikelets’ show only two (Fig. 3.18B, right). The time required by the large spike to repolarize to half the voltage is two times shorter than that of the spikelets. These differences in voltage kinetics suggest a distinct mechanism contributing to both de- and repolarization of the two types of spikes. The occurrence of spikes with distinct properties in a single granule cell was recently reported in the frog olfactory granule cells (Zelles *et al.*, 2006). In this particular study, the somatic spikelets were related to active events occurring at granule cell dendrites based on their temporal correlation to localized dendritic [Ca^{2+}] transients (Zelles *et al.*, 2006). The fact that granule cells process both input and output at their dendrites may necessitate their development of unconventional physiological mechanisms that are considerably different from other central neurons.

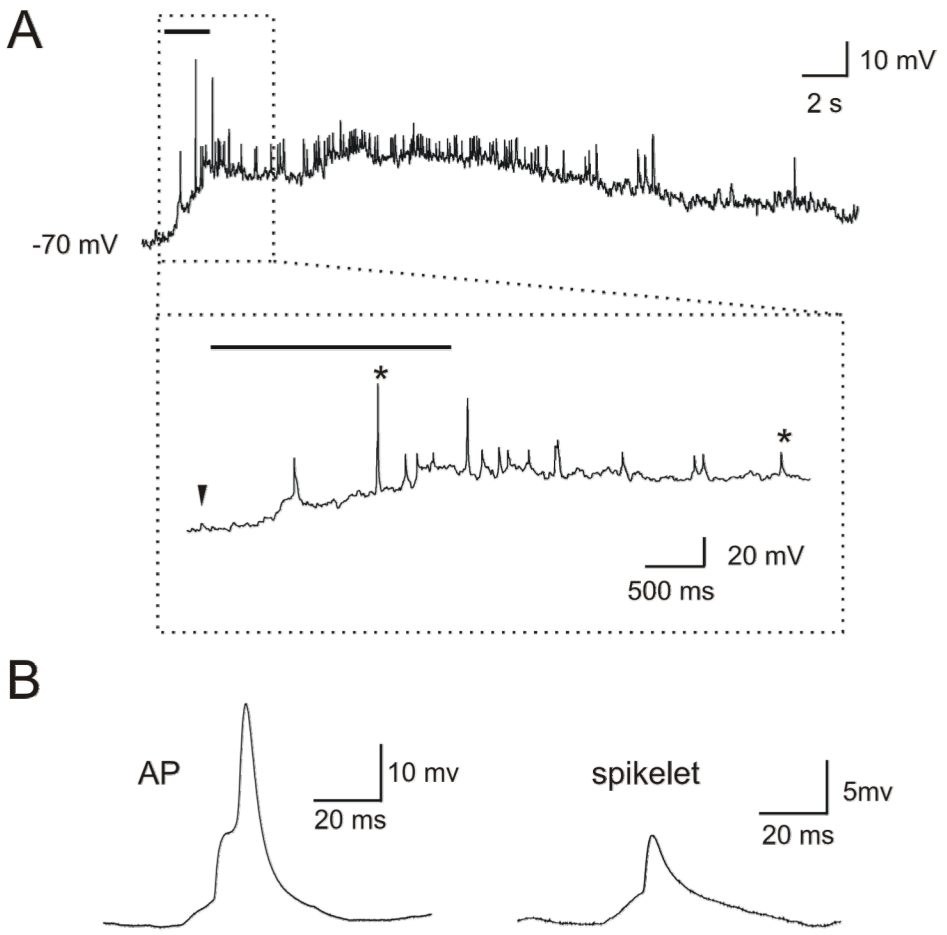

Figure 3.18 Granule cell action potentials and spikelets (A) Odorant stimulation elicit two large spikes and many smaller 'spikelets' in this granule cell. Both types of spikes can be clearly distinguished from EPSPs (arrow) by their larger amplitude and faster kinetics. (B) The large spikes show three steps of integration and a faster repolarization, whereas the 'spikelets' show only two integration steps and a slower repolarization.

3.3 $[Ca^{2+}]_i$ activity in olfactory bulb neurons

Electrophysiological techniques allow a detailed characterization of spiking or subthreshold responses in single neurons. However, a comprehensive analysis of network response requires a method that monitors the neuronal activities simultaneously in a large population of neurons. To this end, $[Ca^{2+}]_i$ imaging has recently emerged as one of the most popular techniques. In the following sections, we applied $[Ca^{2+}]_i$ imaging to characterize the activity of neuronal populations in the olfactory bulb and relate the $[Ca^{2+}]_i$ signals to their electrical activities.

3.3.1 Ongoing $[Ca^{2+}]_i$ fluctuation in MCs and GCs

First, time-series of calcium images were recorded from MCs and GCs (390 cells in 10 slices; 186 MCs and 204 GCs) without odorant stimulation. In both cell types, we observed prominent ongoing $[Ca^{2+}]_i$ fluctuations consisting of pulses with fast increases followed by slower decays. Amplitudes and frequencies of the fluctuations varied from cell to cell as exemplified by the traces shown in Fig. 3.19.

To estimate the $[Ca^{2+}]_i$ levels in these cells, we performed ratiometric measurements of fura-2 fluorescence. The calibration parameters (R_{min}, R_{max}, K_d) were obtained in separate experiments where single cells were loaded with defined concentration of fura-2 and calcium (see Methods). The fluorescence background in bulk-stained slices was estimated *in-situ* for each cell using a pixel-based algorithm (Chen *et al.*, 2006). With the calibration parameters and fluorescence background values in each excitation wavelength, we converted the ratio of the fluorescence intensities excited at

351 and 382 nm to the absolute $[Ca^{2+}]_i$ (Grynkiewicz *et al.*, 1985). In MCs, the intracellular $[Ca^{2+}]_i$ was estimated to fluctuate between 50 nM and a few µM (n = 10; Fig. 3.20A). In contrast, the estimated $[Ca^{2+}]_i$ in GCs was much lower, being in the range from 20 to several hundreds of nM (n = 10; Fig. 3.20B).

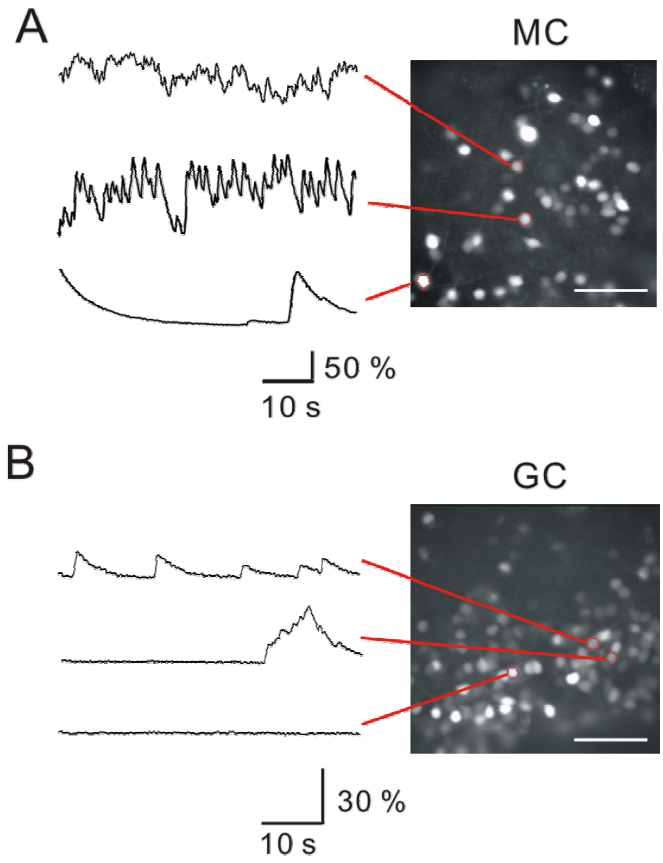

Figure 3.19 Spontaneous $[Ca^{2+}]_i$ activities in mitral and granule cells Sequence of fluorescence images were recorded in the absence of stimulation. Many cells in the mitral cell layer (A) and in the granule cell layer (B) show spontaneously occurring $[Ca^{2+}]_i$ fluctuations.

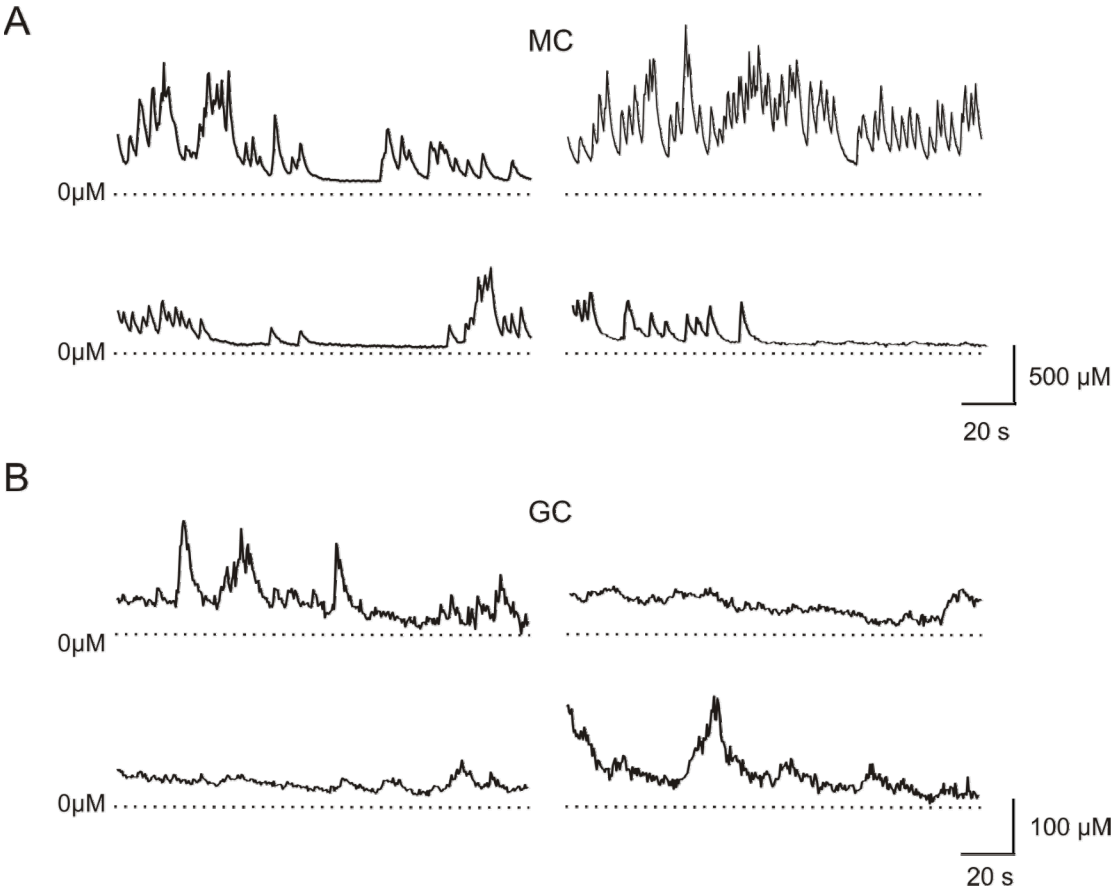

Figure 3.20 Quantification of $[Ca^{2+}]_i$ in bulbar neurons (A) Mitral cells show $[Ca^{2+}]_i$ fluctuations in the range of ~50 nM to a few µM. (B) $[Ca^{2+}]_i$ in granule cells is much lower, being in the range of ~20 nM to several hundred nM.

To quantify the frequency of ongoing $[Ca^{2+}]_i$ fluctuations, we took the rising phases of the fluctuations (Fig. 3.21A; marked in red), and calculated the proportion of the rising periods to the total recording time, which we denominated “mean activity index” (MAI) (see Method). On average, MCs showed higher MAI than GCs (Fig. 3.21B). According to the cumulative probability plot, approximately 90 % of MCs showed substantial $[Ca^{2+}]_i$ fluctuations (MAI > 0.05), while only 46 % of GCs displayed the same level of fluctuations (Fig. 3.21C). In addition, highly active cells (MAI > 0.26) were exclusively located in the mitral cell layer resulting in a broader distribution of $[Ca^{2+}]_i$ activity levels in MCs than in GCs (Fig. 3.21C). Taken together, while both MCs and GCs showed ongoing $[Ca^{2+}]_i$ activities, the MC population displayed a broader activity level distribution than the GC population.

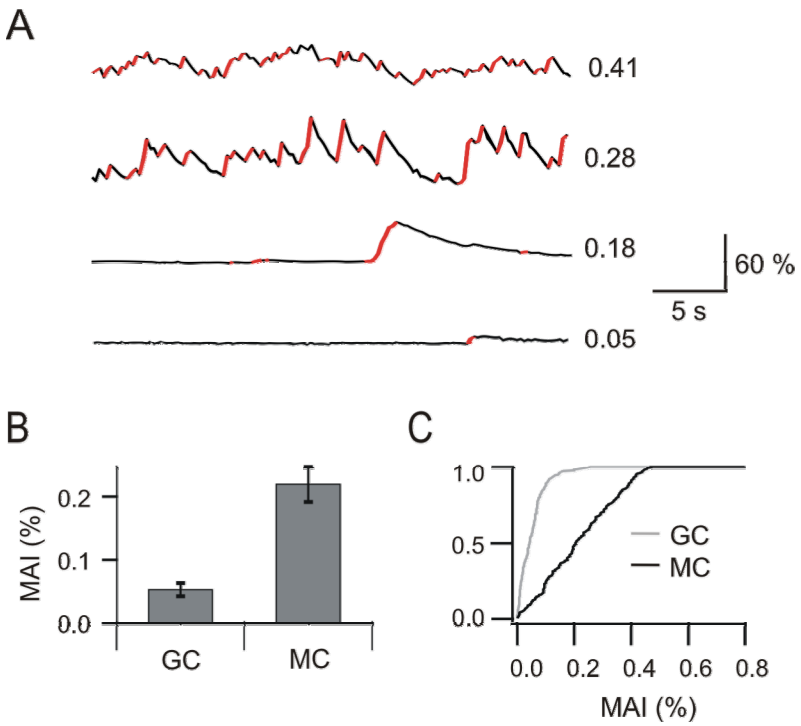

Figure 3.21 Mean activity index (MAI) of mitral and granule cells (A) Mean activity indices (MAI) are shown to the right of each trace. (B) Ongoing $[Ca^{2+}]_i$ fluctuations in populations of MCs and GCs were quantified using MAI. The averaged MAI of MCs (0.219 ± 0.009, n=186)

is significantly higher than that of GCs (0.053 ± 0.003, n=204). (C) MAI in MCs shows a broader distribution (range: 0-0.5) than that in GC (range: 0 to 0.26). All data are shown as (mean ± s.e.m)

We next examined the $[Ca^{2+}]_i$ source underlying the generation of the observed ongoing $[Ca^{2+}]_i$ fluctuations. First, when the normal Ringer's solution (2 mM $[Ca^{2+}]$) was replaced by calcium-free Ringer's solution, $[Ca^{2+}]_i$ fluctuations ceased and dropped to a very low level (n = 28 cells in 2 slices; Fig. 3.22A), suggesting that the spontaneous $[Ca^{2+}]_i$ fluctuation requires calcium influx from the extracellular space. Second, ongoing $[Ca^{2+}]_i$ fluctuations in most cells were blocked by applying TTX (1 μM) to the slice (n = 42 cells in 3 slices; Fig. 3.22B), suggesting the $[Ca^{2+}]_i$ fluctuations of most cells depend on the activation of voltage-gated sodium channels in the slice. Finally, the nonspecific voltage-activated calcium channels blocker cadmium (200 μM) also suppresses ongoing $[Ca^{2+}]_i$ fluctuations (n = 21 cells in 2 slices; Fig. 3.22C), suggesting that the VACCs are one of the calcium sources underlying the observed $[Ca^{2+}]_i$ fluctuations.

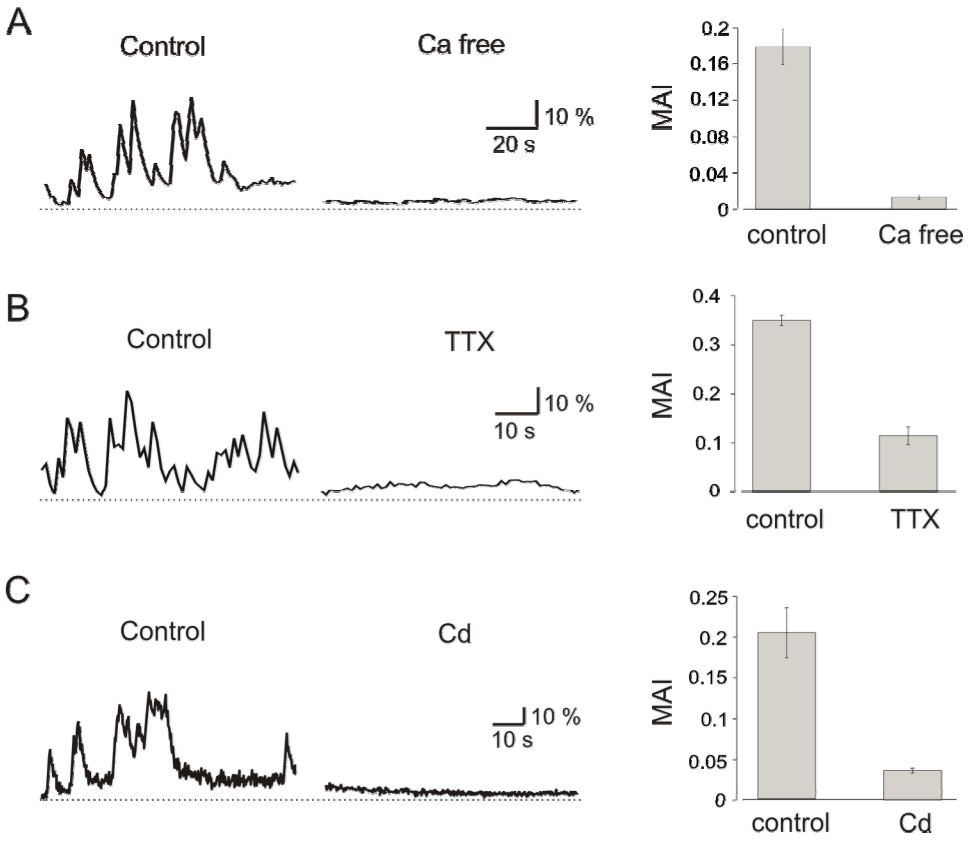

Figure 3.22 $[Ca^{2+}]_i$ sources of spontaneous $[Ca^{2+}]_i$ fluctuation (A) Bath perfusion of calcium free Ringer's solution blocked the spontaneous $[Ca^{2+}]_i$ fluctuations. (B) Bath application of TTX blocked $[Ca^{2+}]_i$ fluctuations in most cells. (C) Spontaneous $[Ca^{2+}]_i$ fluctuations are also blocked by the non-specific VACC blocker cadmium.

3.3.2 Odor modulation of the ongoing $[Ca^{2+}]_i$ activity

To investigate odor-evoked $[Ca^{2+}]_i$ responses in bulbar cells, short pulses of odorant solution were applied to the olfactory epithelium while sequences of images were taken from the OB (see Methods). As a number of cells exhibited substantial ongoing $[Ca^{2+}]_i$ activities, it was often hard to determine whether a particular $[Ca^{2+}]_i$ transient following stimulation was a stimulus-evoked response or part of the ongoing activity. To clearly establish odor-

evoked responses, we used a recording protocol in which spontaneous activity was recorded for one minute, and then the repeated stimuli were applied at the beginning of the second, third, and fourth minute. Though responses to repeated stimuli varied to a certain extent, they shared a common temporal pattern (Fig. 3.23).

In MCs (10 slices, 226 cells), odorant stimulation modulated the spontaneous $[Ca^{2+}]_i$ activity in at least three different ways (Fig. 3.23A). Odor could elicit either an increase of $[Ca^{2+}]_i$ (Fig. 3.23A d,f,g) or a decreased in $[Ca^{2+}]_i$ (Fig. 3.23A a,b) with various durations. In the latter cases the cells usually displayed substantial spontaneous $[Ca^{2+}]_i$ fluctuations so that the response appeared as a suppression of the spontaneous activity. In addition, some MCs showed more complex responses consisting of an initial $[Ca^{2+}]_i$ increase followed by suppression of spontaneous fluctuations (Fig. 3.23A c,e,h). The duration of the suppression varied from several seconds to some minutes.

Using the same experimental protocol, we also analyzed odor-evoked $[Ca^{2+}]_i$ responses in GCs (14 slices, 246 cells). The majority of GCs showed response waveforms consisting of single or compound $[Ca^{2+}]_i$ transients with different durations (Fig. 3.23B i-n). Suppressive responses in GC appeared to be much fewer.

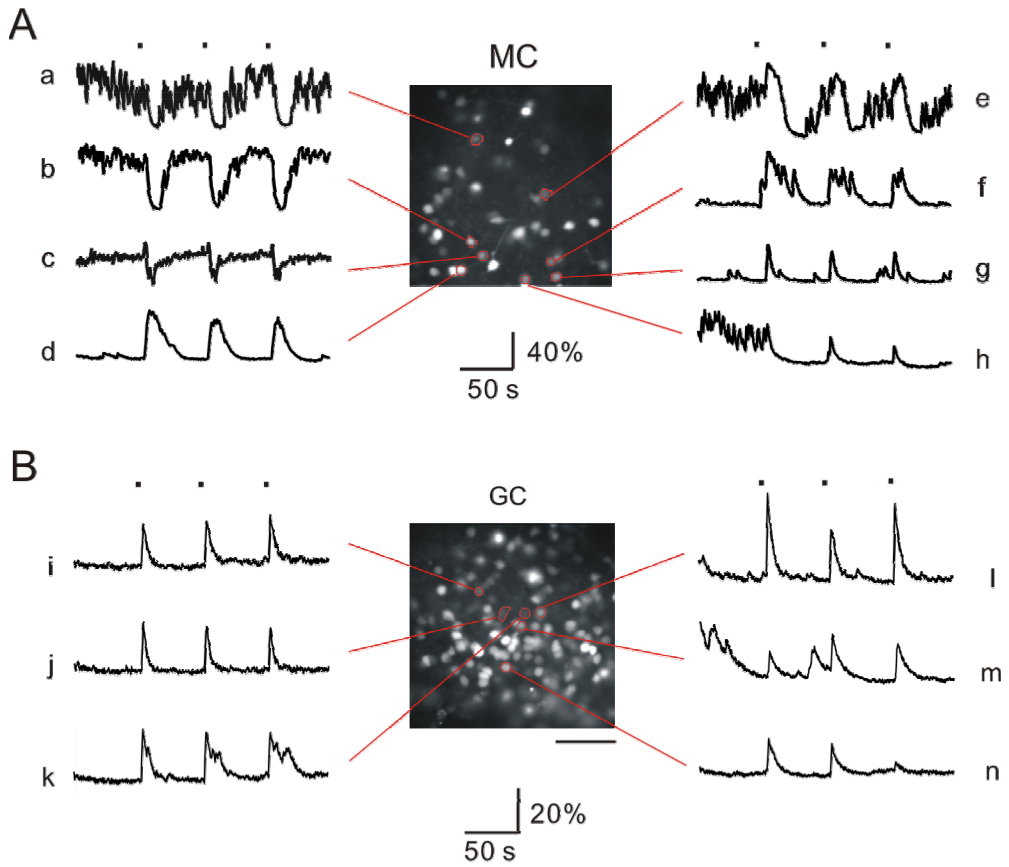

Figure 3.23 Odors induce somatic $[Ca^{2+}]_i$ dynamics in MCs and GCs. (A) MCs show diverse odor-evoked responses of increases (d,f,g) or decreases (a,b) in $[Ca^{2+}]_i$. In some cases, $[Ca^{2+}]_i$ increases initially and then decreases to a level lower than the pre-stimulus level (c,e). (B) A majority of GCs respond to odorant stimulation as a stereotyped $[Ca^{2+}]_i$ waveform consisting of a $[Ca^{2+}]_i$ rise followed by a decay to the pre-stimulus level (i-n). Odorant stimulations were indicated by the thick bars above the fluorescence traces.

To summarize the responses of all cells imaged, we represent the response waveform of each cell as a horizontal colored bar using a color spectrum from blue (low $[Ca^{2+}]_i$) to red (high $[Ca^{2+}]_i$) (Fig. 3.24). Clearly, suppressive $[Ca^{2+}]_i$ responses occurred more frequently in MCs (56 %) than in GCs (15 %). Moreover, among the MCs showing an odor-induced decrease in $[Ca^{2+}]_i$, many displayed a complex response waveform where the decrease was preceded by a short $[Ca^{2+}]_i$ increase (Fig. 3.24).

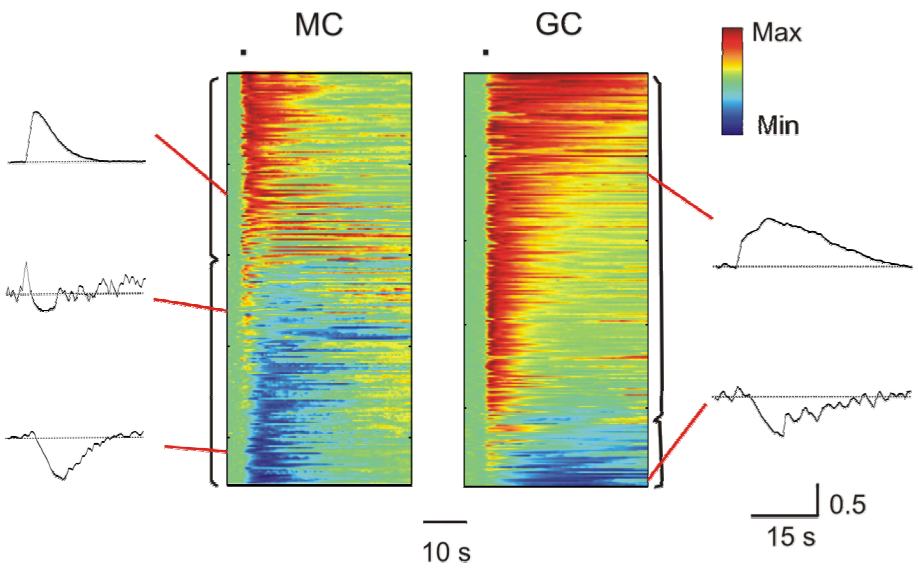

Figure 3.24 Summary of the odorant induced $[Ca^{2+}]_i$ response in 226 MCs and 246 GCs. The fluorescence trace of each cell is displayed as a color coded bar. Mitral cells show odorant induced $[Ca^{2+}]_i$ decreases more often than granule cells.

3.3.3 Spatial distribution of responsive mitral cells

To investigate how MCs that show increasing or decreasing $[Ca^{2+}]_i$ responses were distributed spatially, we generated response maps by marking a responding cell in red or in blue if it showed an increasing or decreasing response, respectively. Response maps of four different bulbs are shown as examples in Fig. 3.25A. From these maps, we did not observe an obvious spatial segregation between the two types of responding cells. That is, the cells with similar response properties do not appear to strictly segregate into 'columns', as often observed in visual or somatosensory cortical areas. Rather, the cell bodies of increasing (red) and decreasing (blue) cells appeared to be intermixed and, in some cases, could even be

adjacent to each other. The non-responding (unmarked cells) cells were also intermingled with the responding cells.

To further quantify these spatial data, we compared the distance of a responding cell to its nearest responding cell of the same type and to its nearest responding cell of the other type. Despite the lack of a strict spatial segregation between these two types of responding cells, we found that the average distance from a given cell to the nearest responding cell of the same type is significantly shorter than that to the nearest responding cell of the other type. For example, the distance from a given increasing cell (98 cells in 7 bulbs tested) to its nearest increasing cell (D_{ii}, 21 ± 1.3 μm) was significantly shorter than that to its nearest decreasing cell (D_{id}, 38 ± 2.3 μm; paired t-test, $p < 0.005$; Fig. 3.25B). The same is also true for decreasing cells (79 cells in the same seven bulbs; D_{dd} = 18 ± 1.2 μm and D_{di} = 29 ± 1.8 μm; paired t-test, $p < 0.005$). This indicates that the cells of the same response type tend to be closer to each other than the cells of different response type.

Consistent with these results, when we compare the response identity of a given cell to that of its nearest responding cell, in 68% of cases, the cell respond in the same way (increase or decrease) as its nearest responding neighbor, suggesting certain degree of response clustering. However, in the remaining 32% cases, neighboring responding cells show an opposite response, emphasizing a substantial intermix of the two populations. Taken together, these result shows that mitral cells with similar response properties have certain tendency to be located in a spatial neighborhood but at the same time extensively intermingle with cells of opposite response characteristics.

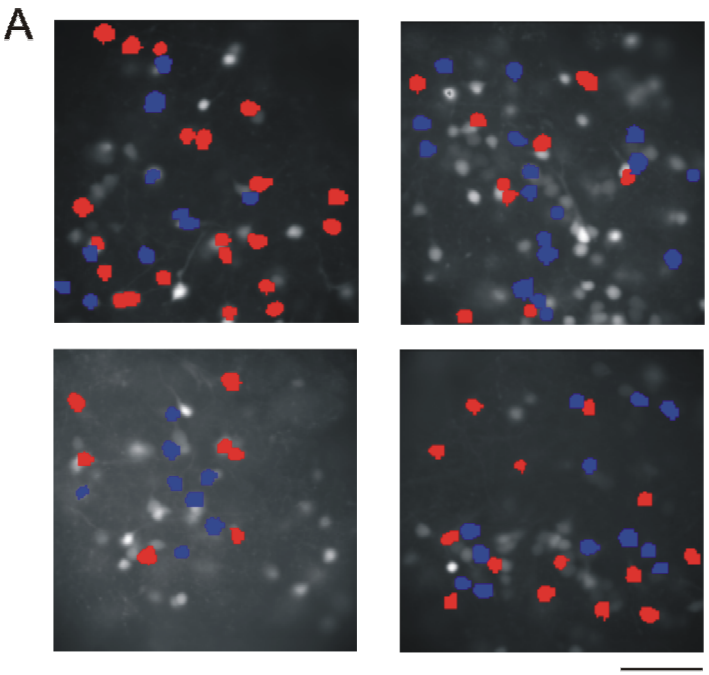

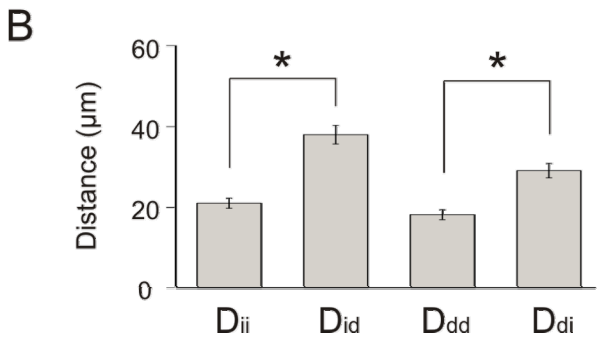

Figure 3.25 Spatial distribution of responsive mitral cells (A) MCs showing a $[Ca^{2+}]_i$ increase in response to odorant stimulation (masked in red) were spatially intermingled with MCs showing $[Ca^{2+}]_i$ decrease (masked in blue). (B) The distance from a given increase cell to the nearest increase cell (D_{ii}) is significantly shorter than its distance to the nearest decrease cell (D_{id}). Similarly, the distance from a given decrease cell to the nearest decrease cell (D_{dd}) is also significantly shorter than its distance to the nearest increase cell (D_{di}). $p<0.005$ in both cases. Scale bar: 50µm in (A)

3.4 $[Ca^{2+}]_i$ – spike relationship

To investigate the relationship between somatic $[Ca^{2+}]_i$ and electrical activity, we recorded both activities simultaneously using calcium imaging and on-cell loose patch recording with and without odorant stimulation. During the ongoing $[Ca^{2+}]_i$ fluctuations in MCs, $[Ca^{2+}]_i$ increases mostly coincided with the occurrence of action potentials (Fig. 3.26). A quantitative relationship between $[Ca^{2+}]_i$ increases and the number of action potentials was derived as follows (i) we calculated the ratio (r) of the background-corrected fluorescence values taken at 351 and 382 nm excitation (Fig. 3.26A, upper panel, along with action potentials); (ii) the change of $[Ca^{2+}]_i$ were then shown as ratio differences (dr) in a sliding window of 400 ms (Fig. 3.27A, middle panel), and (iii) action potentials were counted within the same time intervals (Fig. 3.27A, lower panel). dr (t) and the spike count clearly showed a high correlation, which is also evident when dr is plotted as a function of the corresponding spike numbers (Fig. 3.27B). In this case, the correlation coefficient ρ between dr and spike numbers was ρ=0.83. This linear relationship was found in all cells sampled in the mitral cell layer, whereby dr /spike varied from cell to cell (Fig. 3.27C).

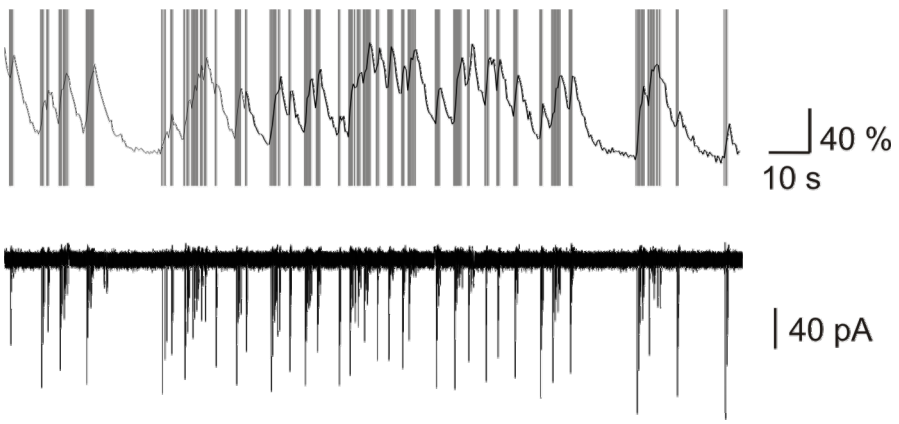

Figure 3.26 Action potentials occur coincidently with the rising periods of $[Ca^{2+}]_i$ fluctuations in MCs. The timings of action potentials were detected and displayed as vertical lines superimposed on the $[Ca^{2+}]_i$ trace of the same cell recorded simultaneously.

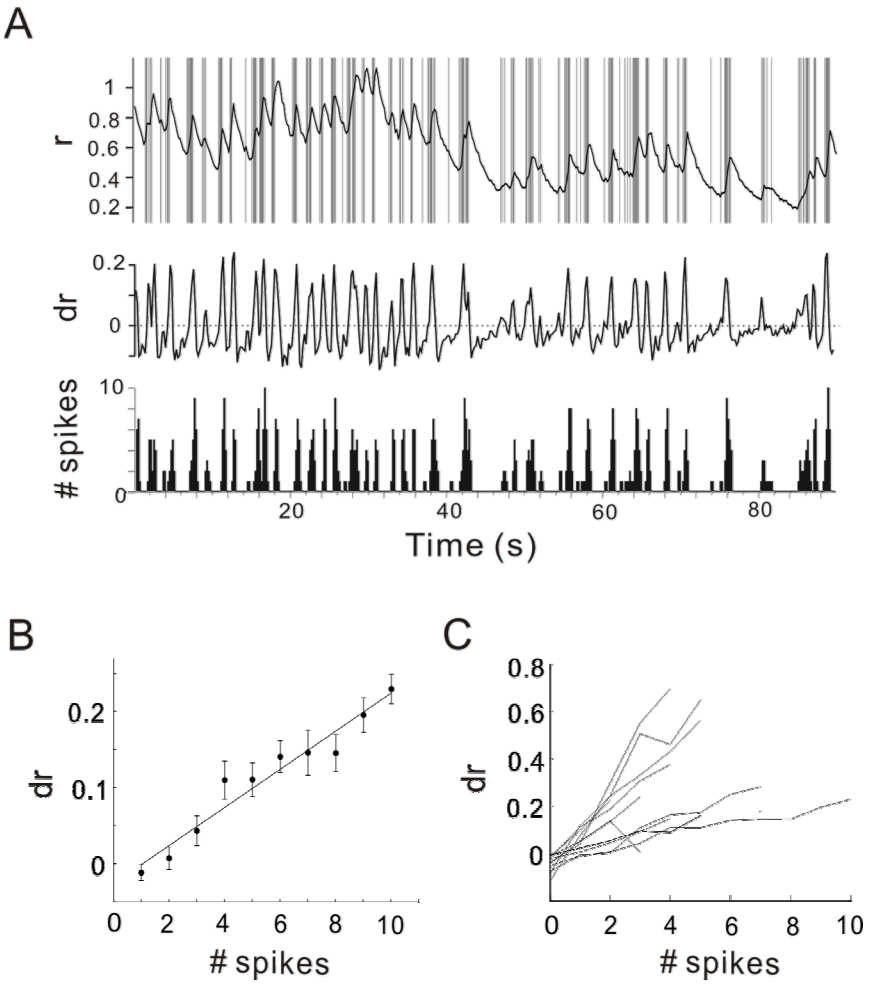

Figure 3.27 Quantitative relationship between spikes and $[Ca^{2+}]_i$ (A) The increases of the $[Ca^{2+}]_i$ were highlighted by the first derivatives of ratios (dr) above zero (middle). The $[Ca^{2+}]_i$ increases (dr > 0)and APs occur coincidently. (B) Amplitudes of dr are highly correlated with the numbers of spikes. (C) Summary of this relationship in all MCs sampled (n = 12).

When the same measurement and evaluation procedures described above for MCs were done on GCs, we obtained markedly different results. In the majority of the GCs sampled, increases in $[Ca^{2+}]_i$ did not appear to be highly related to the occurrence of action potentials. On the other hand, we also observed numerous action potentials without associated $[Ca^{2+}]_i$ increases (Fig. 3.28). The degree of correlation varied from cell to cell as exemplified in Fig. 3.28.

Fig. 3.28 gives example traces with the corresponding ρ values from MCs and GCs. Traces with larger values of ρ showed a high correlation between $[Ca^{2+}]_i$ increases and action potentials, while traces with smaller values of ρ were characterized by a large number of uncorrelated events. While all MCs recorded showed a high correlation between $[Ca^{2+}]_i$ increases and action potentials ($\rho = 0.68 \pm 0.03$, n=12), the average correlation in GCs was significantly lower ($\rho = 0.37 \pm 0.05$, n=15; Fig. 3.28B).

To investigate how different categories of odorant-induced calcium responses were related to electrical responses, we first imaged a population of neurons and then targeted a responsive cell for simultaneous on-cell patch clamp and calcium imaging.

The result of these simultaneous recordings in mitral cells showed a high correlation between $[Ca^{2+}]_i$ response waveforms and odor-evoked spiking patterns. Whenever an odorant elicited a $[Ca^{2+}]_i$ increase, there were action potentials coinciding with the rising phase of the $[Ca^{2+}]_i$ signal (Fig. 3.29A). On the other hand, when an odorant led to a decrease in $[Ca^{2+}]_i$, a corresponding suppression of firing was observed (Fig. 3.29B). Thus in MCs, $[Ca^{2+}]_i$ could reflect both excitatory and inhibitory spike activities during sensory stimulation. Taken together, $[Ca^{2+}]_i$ and spike activity in MCs appeared to be highly correlated during both spontaneous and odor-evoked activity.

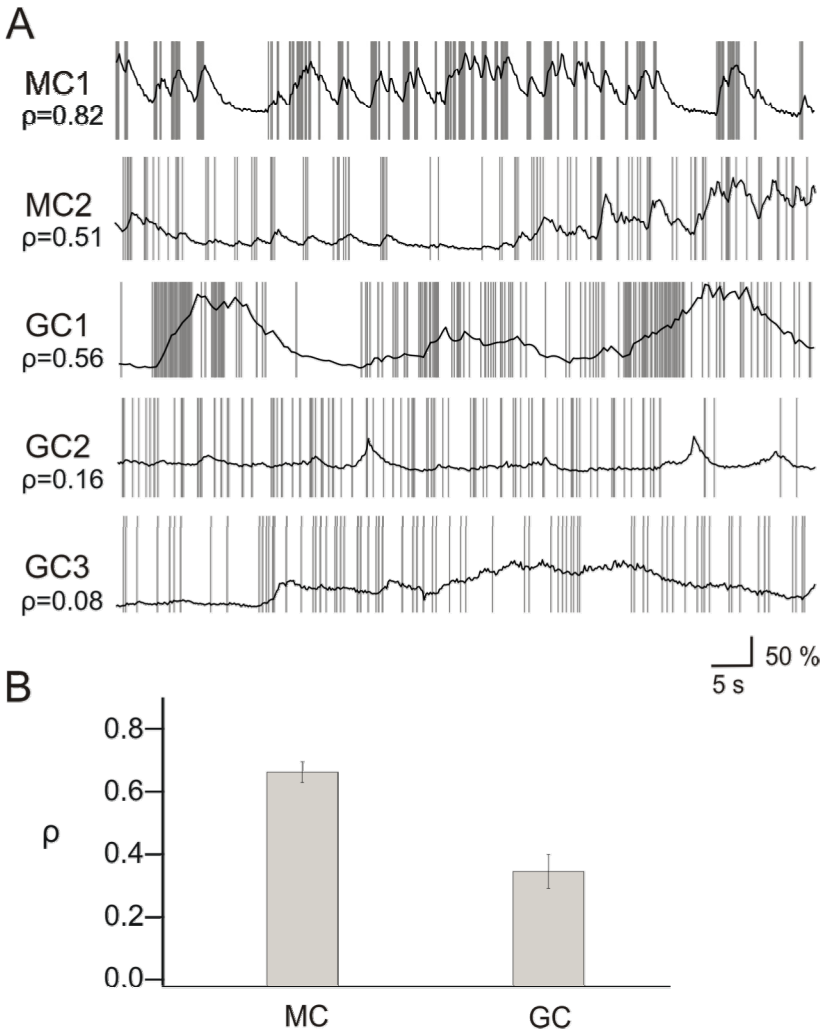

Figure 3.28 GCs show lower correlations between action potentials and $[Ca^{2+}]_i$ than MCs. (A) Examples of simultaneous electrical and $[Ca^{2+}]_i$ recording in MCs and GCs. Correlation coefficients (ρ) between ⅆr and spike numbers were calculated for each record. (B) Correlation coefficients (ρ) between AP number and ⅆr is significantly lower in GCs than in MC (t-test, $p<0.0005$).

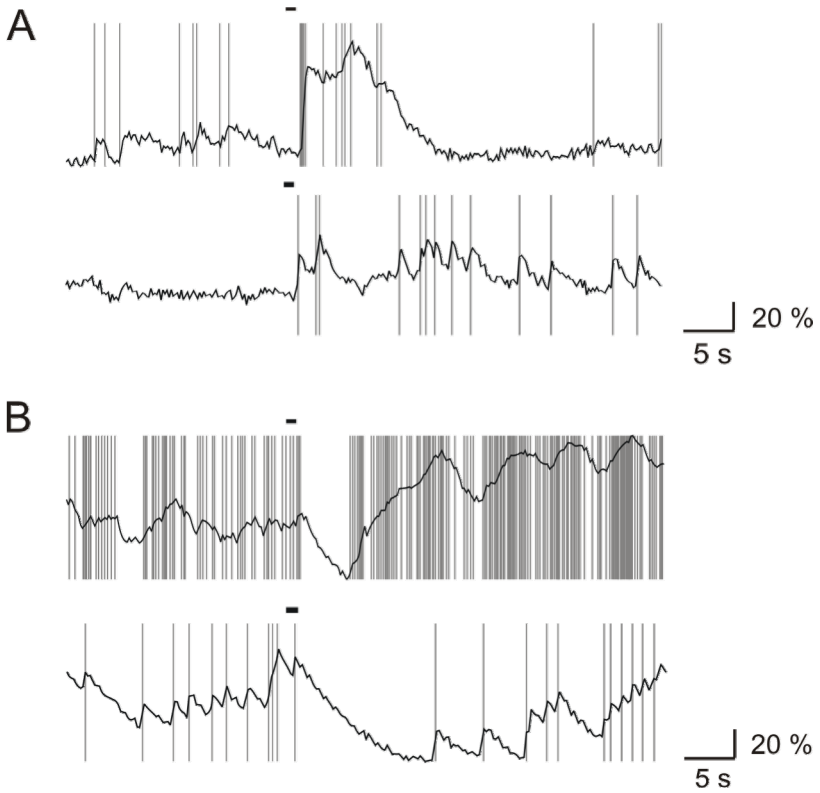

Figure 3.29 Relationship between odor-evoked $[Ca^{2+}]_i$ responses and spikes in MCs. (A) Odor-elicited spikes coincide with the rising phases of the $[Ca^{2+}]_i$ responses (B) When MCs show a decrease in somatic $[Ca^{2+}]_i$, they also exhibit a suppressive spiking pattern upon odorant stimulation. Note that these cells often show prominent spontaneous $[Ca^{2+}]_i$ fluctuations and ongoing spikes.

When $[Ca^{2+}]_i$ was sampled at relatively low image acquisition rate, the rising phase of $[Ca^{2+}]_i$ responses appeared to be rather smooth. In order to distinguish whether this was due to a high calcium buffering capacity brought about by the introduced fluorescence indicator or, alternatively, to the low acquisition rate, we performed experiments at a faster imaging rate (667 Hz) using the line scanning mode of the LSM510. At this rate, we were able to resolve discrete stepwise $[Ca^{2+}]_i$ increments during the increasing phase of $[Ca^{2+}]_i$ response (Fig. 3.30A). By simultaneous on-cell recordings from individual MCs and fast CCD recording (a single pixel; 125 Hz), we observed

a precise correlation between $[Ca^{2+}]_i$ steps and individual spikes (Fig. 3.30B). Each spike within the odor-evoked burst corresponded to a step-like $[Ca^{2+}]_i$ increment. Fast $[Ca^{2+}]_i$ imaging can thus resolve $[Ca^{2+}]_i$ steps induced by individual spikes.

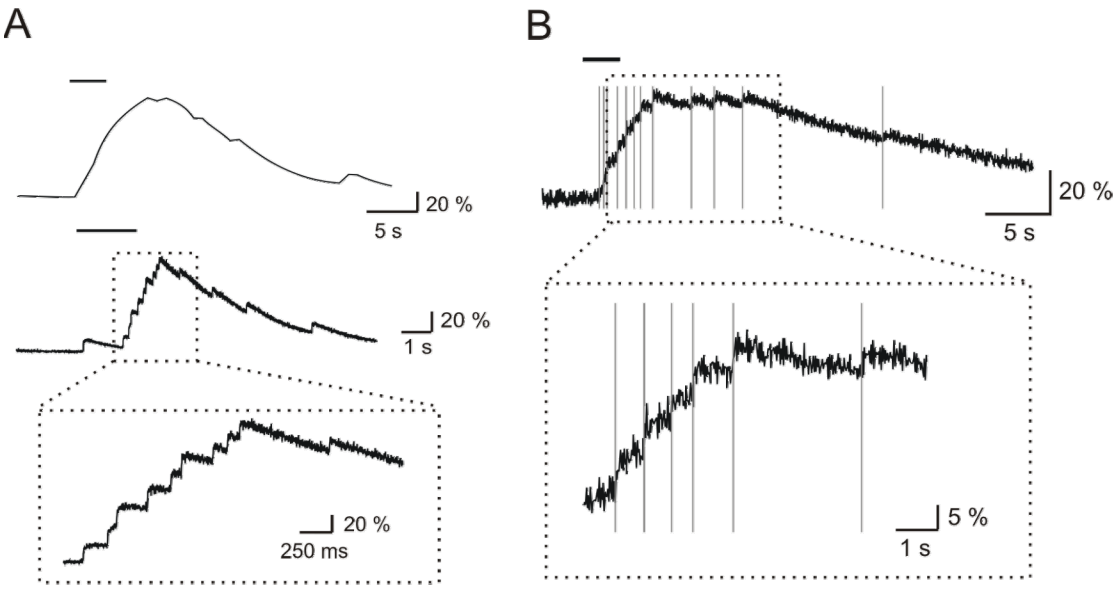

Figure 3.30 Odorant induced stepwise calcium increase tightly correlated to action potentials (A) Fast calcium imaging using line scanning mode of a confocal microscope resolves distinct stepwise $[Ca^{2+}]_i$ increments during odorant-induced $[Ca^{2+}]_i$ response. (B) The stepwise $[Ca^{2+}]_i$ increments precisely correlate to the occurrence of individual spikes. Odorant stimulation is indicated as a horizontal bar above each trace.

In GCs, the relationship between odor–evoked $[Ca^{2+}]_i$ dynamics and spiking activity appeared to be more complex. In some cells, (e.g. Fig. 3.31 A), the increasing phase of an odorant-evoked $[Ca^{2+}]_i$ response coincided with the occurrence of action potentials (Note in this cell, however, several spontaneous spikes failed to generate an observable $[Ca^{2+}]_i$ transients while other spikes do). In other cells, (e.g. Fig. 3.31B), odorant-induced spikes were only partly correlated with the rising phase of $[Ca^{2+}]_i$ responses, and a substantial number of spikes occurred at the falling phase of the $[Ca^{2+}]_i$ signal. Some of these cells even showed $[Ca^{2+}]_i$ increases but a suppression of their spontaneous spiking activity (Fig 3.31 C).

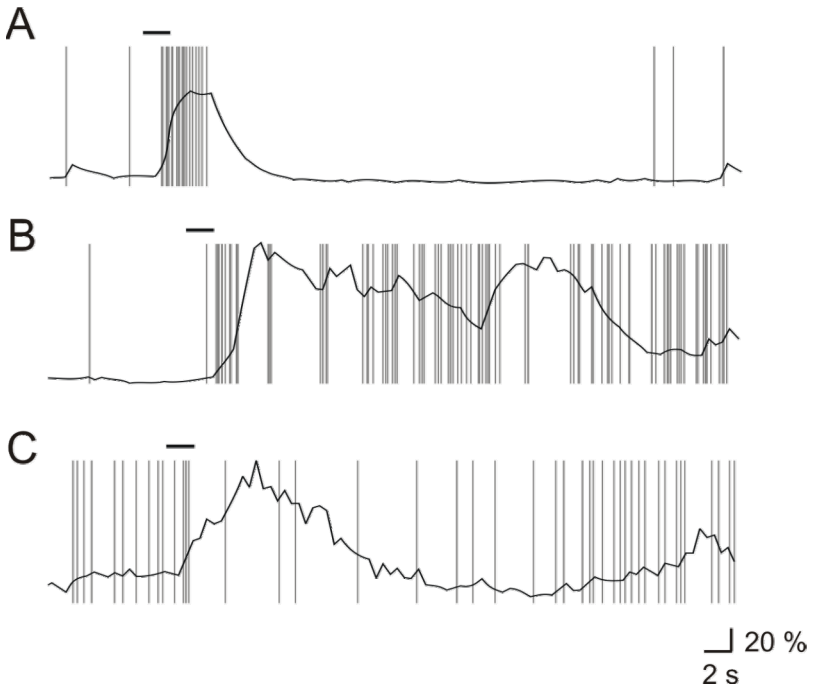

Figure 3.31 Odor-evoked $[Ca^{2+}]_i$ responses and spikes in GCs are less correlated than in MCs. (A,B) In most GCs, odor-evoked increases in $[Ca^{2+}]_i$ only in part correlate with APs.

(C) Spiking even seems to be suppressed during $[Ca^{2+}]_i$ responses in some neurons.

We further combined on-cell recordings with fast calcium imaging to analyze the correlation between spiking and the fast components of the $[Ca^{2+}]_i$ responses in GCs (Fig. 3.32). In some GCs, fast calcium imaging could resolve desecrate step-like $[Ca^{2+}]_i$ events, which corresponded to the occurrence of single action potentials (Fig 3.32 A). However, we often observed that the $[Ca^{2+}]_i$ could start rising before the occurrence of the first action potential (Fig 3.32 B) or could continue to increase even after the neuron stop firing (Fig 3.32C and D). Moreover, some spikes failed to generate observable $[Ca^{2+}]_i$ signals as other spikes in the same neuron do (Fig 3.32 A and C). Taken together, both ongoing and odor-evoked somatic $[Ca^{2+}]_i$ dynamics are highly correlated to the spiking activity in MCs whereas they are not well related to the occurrence of spikes in GCs.

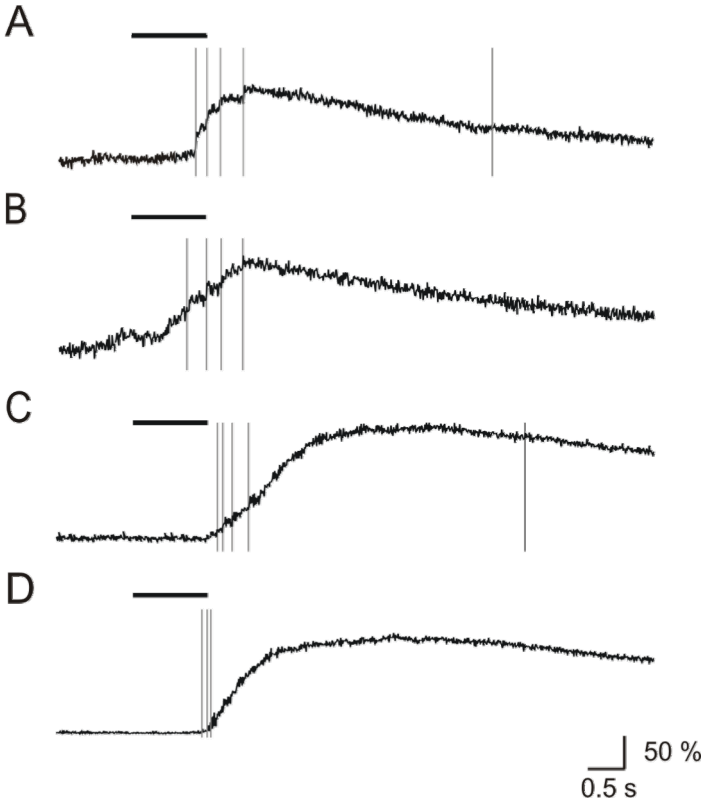

Figure 3.32 Fast recording of GC spike and [Ca2+]$_i$. (A) Only a subset of spikes correspond to step-like [Ca^{2+}]$_i$ increments during odorant stimulation. (B) [Ca^{2+}]$_i$ increase precede the occurrence of the first AP (C,D) Smooth and prolonged [Ca^{2+}]$_i$ increases were observed after the neuron stop firing.

4. Discussion

4.1 Spontaneous electrical and $[Ca^{2+}]_i$ activity in the olfactory bulb

This work shows that the olfactory bulb of a tadpole nose-brain preparation generates a variety of spontaneous electrical and $[Ca^{2+}]_i$ activities. Moreover, the ongoing activity can be modulated by sensory input in various ways. Viewing this fact from a different perspective, the responses of olfactory bulb neurons can be considered as occurring in a rich context of ongoing activity, which may help to explain the complete meaning of the stimulus response. Thus, the characterization of network activities in the olfactory bulb must take into account the dynamics of its intrinsic activity.

4.1.1 The origin of ongoing activity

In the nose-olfactory bulb preparation spontaneous activity may result from external excitatory drives such as the spontaneous input from olfactory receptor neurons or the top-down input from higher brain centers. Alternatively, the olfactory bulb network may be able to generate its activity by intrinsic mechanisms. For example, the rhythmic activation of membrane conductances may allow single neurons to function as pacemakers, or the recurrent excitatory connection within the network could allow the activities to propagate in loops, thus supporting their maintenance. Such a variety of mechanisms do not contradict each other, and each of them is likely to partly contribute to experimental observations (Hayar *et al.*, 2004; Puopolo *et al.*,

2005). Indeed, spontaneous activities persist in the isolated OB preparation where the inputs from olfactory receptor neurons were removed, suggesting that the intrinsic bulbar mechanisms may be sufficient for ongoing activities (Hayar *et al.*, 2005; Heinbockel *et al.*, 2004; Bardoni *et al.*, 1995). However, this does not exclude the possible modulatory roles of receptor neurons because it has been reported in frog olfactory bulbs that the spontaneous spiking rate in MCs become significantly higher after the removal of receptor inputs (Rospars *et al.*, 1994).

4.1.2 Bursting activity and $[Ca^{2+}]_i$ fluctuations in MCs

One of the most prominent features of the ongoing activity in MCs is that they often fire in burst. Each burst usually consists of ~ 2 to10 subsequent action potentials with an intra-burst interval of 30 to 40 ms (Fig. 3.8). The intense firing within a burst leads to an accumulation of $[Ca^{2+}]_i$, which manifests itself in the calcium imaging signal as rising phases of ongoing $[Ca^{2+}]_i$ fluctuations (Fig. 3.26). This strict coincidence of bursting action potentials and $[Ca^{2+}]_i$ increases suggests interdependency between these two activities. As small-conductance calcium-activated potassium channels (SK) are proved functionally present in mitral cells of mice (Stoker & Pedarzani, 2000; Maher & Westbrook, 2005), we speculate that they may contribute to regulate the bursting behavior in MCs. Because bursts in MCs are associated with $[Ca^{2+}]_i$ increases, accumulation of $[Ca^{2+}]_i$ within a burst activates SK channels, thereby dampening action potential bursts (Hille, 2001). The SK channel-specific blocker apamin can increase the frequency of repetitive firing elicited by injecting depolarizing current into MC somata (Maher & Westbrook, 2005). If strong excitation triggers bursts in MCs, the elevation of $[Ca^{2+}]_i$

during a train of action potentials will activate SK channels and further suppress spiking.

4.1.3 Decrease of action potential amplitudes within a burst

We regularly observed that the amplitudes of AP-induced currents recorded in on-cell configuration decreased progressively within a burst in MCs (Fig. 3.8). In on-cell patch clamp measurements, the detected currents reflect the capacitive coupling between the intracellular membrane potential and the recording pipette via the small patch of membrane. Thus, the peak values of the induced currents correspond to the maximum instantaneous rate of intracellular potential change during action potentials, while the amount of integral charges reflects the size of the depolarization. We have shown that both peak amplitudes and the integrals of the AP-induced current decreased significantly within a burst, indicating that the slope of intracellular action potential depolarizations are less steep and the amplitudes of action potentials are smaller within a burst.

This interpretation is further supported by whole-cell recording data obtained in bursting mitral cells (Fig. 3.10). In the on-cell configuration, this cell fires in bursts consisting of 2-3 action potentials with decreasing amplitudes (Fig. 3.10A, inset). After breaking into the whole-cell configuration, we observed that the cell showed large (10 to 30 mV) subthreshold membrane potential oscillations (Fig. 3.10B) superimposed by a big spike at the beginning followed by several smaller and slower spikes (Fig. 3.10B, inset). Unlike the large depolarizing phase in the first spike, latter spikes initiated from a much higher membrane potential and reached a smaller voltage, thereby having a much smaller overall depolarization. In addition, the

depolarization kinetics of the second spike is much slower than the first one, consistent with the interpretation that these spikes may correspond to the spikes with decreasing amplitudes observed during the on-cell configuration.

4.1.4 Possible functions of bulbar ongoing activities

Conventionally, spontaneous activities are considered as neuronal 'noise' that contributes to the variability of stimulus responses and must be 'averaged out' by the higher brain regions that read the neural code. However, recent evidence suggests that instead of being completely random, ongoing network activities are highly structured and their dynamics could reflect the underlying network circuitry (Meister *et al.*, 1991; McCormick *et al.*, 1995; Yuste *et al.*, 1995). Since a constantly active circuit has to be maintained at a high metabolic cost, this raises the interesting question what specific function and advantages can ongoing activity provide?

One of the possible functions of ongoing activities in the olfactory bulb is that it may allow the bulbar inhibitory responses to be passed to the next processing stage. Because neurons can conduct action potentials for a long distance without decline, action potentials are used by the projecting neurons to transfer sensory information to other brain regions. Since the only information that matters to a higher brain center is the spiking output of projecting neurons, an inhibitory response of subthreshold hyperpolarization will not be seen directly by the neurons in the next stages. However, a continuously active projecting neuron can 'encode' the local bulbar inhibition as a decrease in their spontaneous firing rate, whereas a neuron that is silent at rest has no way to convey its inhibitory response to its down stream targets.

Like a context in speech helps clarify the meaning of its supporting phrases, the presence of ongoing activity allows to convey inhibitory responses. Thus ongoing activity of mitral cells may be important for higher order neurons to decode the odorant-induced signals in MCs.

In addition to being a context for inhibitory responses, spontaneous activity could have other interesting functions, especially if they drive continuous fluctuations of $[Ca^{2+}]_i$. As $[Ca^{2+}]_i$ is involved in many vital processes such as the regulation of gene expression, synaptic plasticity, and the formation or maintenance of synapses, a high correlation between action potentials and $[Ca^{2+}]_i$ in MCs implies that these processes are eventually activity-dependent. Activity-dependent mechanisms have been suggested to be critically involved in the establishment of precise neuronal connections in many brain regions (Carleton *et al.*, 2003; see review Grubb & Thompson, 2004). In the constantly renewed brain regions such as the olfactory bulb, the high-level of MC spontaneous activity reported here may serve to help newly generated granule or periglomerular cells integrate into a functional bulb circuitry. It has been shown that the spontaneous activities of olfactory receptor neurons are required for the establishment and maintenance of their proper projection pattern (Yu *et al.*, 2004). Whether such mechanisms are important in the olfactory bulb is an intriguing question and awaits further experimental investigation.

4.2 Odor-induced activity in the olfactory bulb

4.2.1 Somatic $[Ca^{2+}]_i$ dynamics reveals both excitatory and inhibitory electrical responses induced by odorant stimulation

Previous calcium imaging studies typically describe the sensory responses of neurons as an increase in their somatic $[Ca^{2+}]_i$ (Ohki *et al.*, 2005; Niell and Smith, 2005). However, when spikes are recorded, it is also known that sensory stimulation can either increase or decrease their firing rates (Hirsch, 2003; Dacey, 1996). If somatic $[Ca^{2+}]_i$ faithfully reports the neuronal electrical activity, it raises the question how inhibitory electrical responses observed commonly in sensory neurons are reflected in their somatic $[Ca^{2+}]_i$ signal. In the olfactory bulb, a system known for its prominent sensory-evoked inhibitory electrical responses (Kauer, 1974; Cang & Isaacson, 2003), we observe a variety of $[Ca^{2+}]_i$ response waveforms including increases, decreases, and a combination of both changes in MCs during natural odorant stimulation (Fig. 3.23A). Decreases of somatic $[Ca^{2+}]_i$ upon sensory stimulation is particularly interesting and has not yet been investigated. To do this, we performed simultaneous recording of action potentials and $[Ca^{2+}]_i$ and show that odorant-induced $[Ca^{2+}]_i$ decreases indeed correspond to inhibitory electrical responses in MCs (Fig. 3.29). Since inhibition of ongoing electrical activities upon sensory stimulation is widely observed in many other brain regions, stimulus-induced decreases in somatic $[Ca^{2+}]_i$ might be a widespread phenomenon and reflect inhibitory electrical responses in neurons that show a high correlation between $[Ca^{2+}]_i$ and spikes.

4.2.2 Spatial patterning of odor responses

Based on their somatic $[Ca^{2+}]_i$ response to a mixture of amino acid, we classified MCs into two response categories and investigated the spatial location of MC somata belonging to either category (Fig. 3.25). Although the response categorization may differ from odorant to odorant, the resulting map

of responses provide some interesting insights into the spatial organization of olfactory bulb output neurons. First, MCs of the same response category can distribute widely in the mitral cell layer, and they are intermixed with or sometimes even adjacent to cells belonging to a different response category. However, further quantitative analysis shows that the intermixed distribution does not imply a complete lack of spatial organization. For example, the average distance from a given cell to the nearest responding cell of the same type is significantly shorter than its distance to the nearest responding cell of the other type, indicating that the MCs responding similarly to amino acids show a certain tendency to be located closer to each other. This intermixed but partial clustering distribution of responsive mitral cells is very different from the spatial organization in the visual and the somatosensory system where cells with similar response properties are closely packed together into columns (Ohki *et al.*, 2005). Our results thus suggest several unique features of olfactory coding (i) local circuits can pick up and transfer very different information, (ii) the olfactory bulb might process similar information in various parts of its circuitry in parallel, and (iii) it might take advantage from distributing its information throughout a large space.

It is worth noting that a surprisingly large proportion (32%) of neighboring mitral cells shows opposite responses ($[Ca^{2+}]$ increase or decrease) to a mixture of amino acids. If we consider the fact that cells responding similarly to a given odorant may respond differently to other odorants, the proportion of neighboring MCs with different odor response profile might be much higher than 32%. Thus, despite the short distance between their somata, a large proportion of neighboring MC can show considerably different response patterns. In the cerebral cortex, neighboring cells showing different response properties can occur only at the border of cortical columns (Ohki *et al.*, 2005).

The reason underlying such different responses in neighboring neurons is their tendency to extent their dendritic tree preferentially to the column they belong to (Katz *et al.*, 1989; Lubke *et al.*, 2003; Kossel *et al.*, 1995). Instead of showing tree-like dendritic structures as in cortical pyramidal neurons, mitral cells receive their receptor inputs in localized tuft structures at the distal part of their primary dendrite. Such anatomical feature makes it much easier for mitral cells to receive highly specific input as compared to cortical pyramidal neurons. This may explain why neighboring cells with different response properties are more common in the olfactory bulb.

4.2.3 Inhibitory responses shaped by dendrodendritic inhibition

Dendrodendritic reciprocal synapses between mitral and granule cells have been suggested to play an important role in olfactory information processing (Woolf *et al.*, 1991; Yokoi *et al.*, 1995; Didier *et al.*, 2001). These synapses could mediate two forms of inhibition. First, the activation of a MC leads to a dendritic glutamate release onto GC spines, thereby resulting in a release of GABA right back onto the activated MC itself, i.e., a feedback inhibition. Second, because a granule cell typically connects to more than one MC (Shipley & Ennis, 1996), it can be activated by a subset of MCs and then exert the inhibitory effect onto other connected MC, thus mediating lateral inhibitions between MCs. Based on the basic circuitry, one can predict that the response of a MC could be an initial excitation followed by inhibition if the feedback dendrodendritic inhibitory pathway is active (Fig. 4.1). Alternatively, MC responses could be purely inhibitory if the cell does not receive direct receptor excitation but is inhibited via the di-synaptic lateral inhibition pathway. Indeed, these two forms of responses are regularly observed in our calcium

imaging data as the most commonly occurring response types in mitral cells (Fig. 3.24), consistent with the simple model based on known OB circuitry. Further confirmation of the involvement of dendrodendritic synapses in shaping MC activity could be obtained either by pharmacological manipulation or by a high-speed recording of the temporal sequence of MC excitatory and inhibitory events.

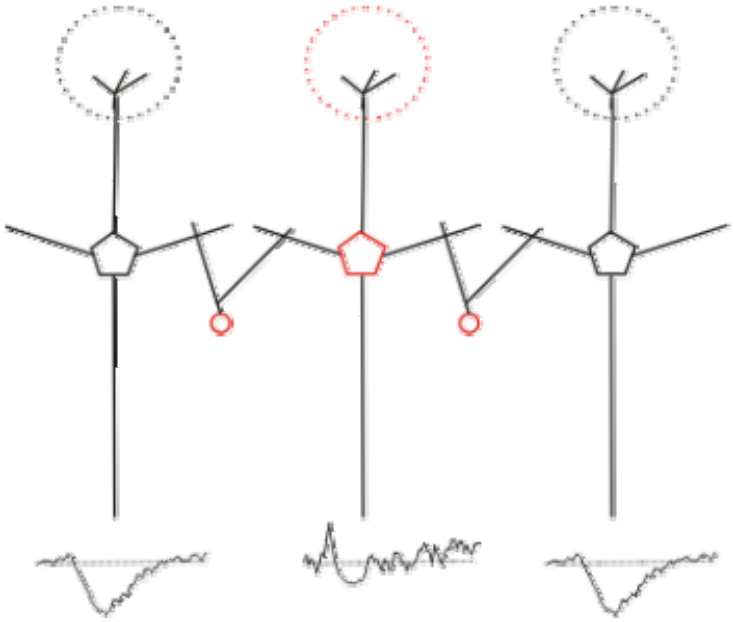

Fig. 4.1 A scheme of the dendrodendritic reciprocal connection between MCs and GCs. The reciprocal connections between glutamatergic MCs and GABAergic GCs could explain the two types of inhibitory responses in MCs. The GCs (red labels) that are activated by the responding MCs to odorant stimulation (label in red) then in turn send inhibitory output back to the responding MC and other MCs connected to these GCs.

4.2.4 Slow currents in MCs underlying the evoked spiking activity

In whole-cell voltage-clamp recordings of odorant-induced synaptic

events, a slow inward or outward current was observed in MCs showing excitatory or inhibitory responses, respectively (Fig. 3.15 and 3.16). The simplest explanation of these currents is that they correspond to a summation of many fast EPSCs or IPSCs. This interpretation, however, would require the current fluctuations during the response being significantly larger than the fluctuation before stimulus, which does not seem to be the case (Fig. 3.15). This suggests that other current sources, such as slow chemical synapses or gap junction-mediated currents may contribute to the odorant induced synaptic currents. In particular, gap junction-mediated current is especially interesting because it has been shown that MCs innervating the same glomerulus are coupled by gap junctions, thereby providing a mechanism for them to synchronize their responses. One possible way to distinguish gap junction-mediated current from chemical synapses mediated input would be checking the voltage dependency of the slow current. In the case of gap junctions, the observed current should not show any voltage dependency whereas currents mediated by an ion channel with certain selective permeability will reverse its direction at the reversal potential. Knowing this may further help to dissect the different input contributions underlying the sensory induced synaptic currents.

4.3 Relationships between somatic $[Ca^{2+}]_i$ and action potentials differ in mitral and granule cells

Somatic $[Ca^{2+}]_i$ has been used to refer neuronal electrical activity based on correlation between $[Ca^{2+}]_i$ and spikes (Mao *et al.*, 2001; Niell and Smith, 2005; Ohki *et al.*, 2005; Sullivan *et al.*, 2005). However, as one of the most important factors governing cell activity and viability, $[Ca^{2+}]_i$ is also known to

undergo complicated regulations that depend on a specific set of molecules a cell expresses (Hartmann and Konnerth, 2005; Bootman *et al.*, 2001; Liljelund *et al.*, 2000). Moreover, the activation of a variety of $[Ca^{2+}]_i$ sources may or may not have causal relationships with action potentials (Denk *et al.*, 1996; Verkhratsky and Petersen, 1998). Thus, it is possible that cells with different $[Ca^{2+}]_i$ handling machineries would have distinct $[Ca^{2+}]_i$-spike relationships.

Herein we demonstrated different relationships between somatic $[Ca^{2+}]_i$ dynamics and the occurrence of action potentials in different cell types. In MCs, $[Ca^{2+}]_i$ increments are precisely correlated with spikes down to the single spike level. Conversely, GCs show a lower degree of correlation and more complex $[Ca^{2+}]_i$–spike relationships. Thus whereas somatic $[Ca^{2+}]_i$ recordings can serve as a powerful tool to detect spikes in MCs as well as in several other cell types (Mao *et al.*, 2001; Smetters *et al.*, 1999; Niell and Smith, 2005), it is not a good indication of APs in GCs. Given the enormous variety of cell types in the central nervous system, such variations in the $[Ca^{2+}]_i$-spike relationship may also happen to occur in other brain regions. Thus, the diversity of neurons must be taken into account when interpreting calcium image data.

4.3.1 Relationship between $[Ca^{2+}]_i$ and spikes in MCs

As revealed by high temporal sampling of the $[Ca^{2+}]_i$ signal, $[Ca^{2+}]_i$ transients in mitral cells are built up by a sequence of discrete increasing steps corresponding to individual action potentials (Fig. 3.30). The precise correlation of individual action potentials and small $[Ca^{2+}]_i$ increments strongly suggests a coupling between these two activities via voltage-activated calcium channels (Markram *et al.*, 1995). Functional voltage-activated calcium

channels have been found in somata of the olfactory bulb mitral cells (Wang *et al.*, 1996; Yunker *et al.*, 2003). These channels are likely to be activated during the depolarization of action potentials, thereby generating transient $[Ca^{2+}]_i$ increases faithfully following each spike.

4.3.2 Relationship between $[Ca^{2+}]_i$ and spikes in granule cells

In contrast to MCs, cells in the granule cell layer show much lower correlations between somatic $[Ca^{2+}]_i$ increases and the occurrence of spikes. Several differences between MCs and GCs may underlie such distinct relationship. First, cell bodies of GCs, different from MCs, show immunoreactivity to T-type LVA calcium channels (Yunker *et al.*, 2003). These channels mediate calcium influx during subthreshold depolarization (Egger *et al.*, 2005). Thus, activation of T-type calcium channels by subthreshold depolarization is likely to contribute to the observed somatic $[Ca^{2+}]_i$ fluctuation in the absence of spikes (Fig. 3.31A,B and 3.32B-D). On the other hand, T-type calcium channels are also known to be fast inactivating at a voltage range similar to that required for its activation (Hille, 2001). In a recent study, the AP-induced $[Ca^{2+}]_i$ transients in GCs are shown to attenuate more than 90 % when the membrane holding potential is changed from –80 to -50 mV (Egger *et al.*, 2003), possibly due to the inactivation of T-type calcium channels. This goes in line with our observation that spikes in GCs often fail to induce observable $[Ca^{2+}]_i$ transients, in particular after odor-induced $[Ca^{2+}]_i$ upstrokes (Fig. 3.28, 3.31, 3.32A,C). Odorant stimulation might drive the GC membrane potential to a more depolarized range (Cang & Isaacson, 2003), which inactivates T-type calcium channels and attenuate spike-evoked $[Ca^{2+}]_i$ transients to an undetectable level.

Another possible explanation for the complex $[Ca^{2+}]_i$–spike relationship in GCs is the activation of somatic NMDA channels. In addition to dendrites (Isaacson and Strowbridge, 1998; Schoppa *et al.*, 1998; Chen *et al.*, 2000), GCs also express functional NMDA channels on their somata (Isaacson and Murphy, 2001). It has been suggested that these channels can be activated physiologically, for example, by the extra-synaptic glutamate spillover from collateral branches of MC axons terminating on the GC basal dendrites (Shepherd, 1972). Calcium influx through NMDA channels may either directly contribute to the observed AP-uncorrelated $[Ca^{2+}]_i$ elevation or may activate Ca^{2+}-dependnt K^+ conductances (Isaacson and Murphy, 2001), leading to a hyperpolarization and suppression of spikes. Thus, somatic NMDA channels may serve as another $[Ca^{2+}]_i$ source adding to the response of somatic $[Ca^{2+}]_i$ increases accompanying by few spikes in GCs.

4.4 Outlook

At high acquisition rates, we often observed that the rising phase of a $[Ca^{2+}]_i$ signal contains step-like $[Ca^{2+}]_i$ increments, which correlate precisely with the occurrence of individual spikes of MCs (see Result and Fig. 3.30). These results suggest the intriguing possibility to use the somatic $[Ca^{2+}]_i$ signal to reconstruct the precise timing of spikes in many neurons recorded simultaneously. This application may be interesting in many neuronal networks, but it is especially interesting in the olfactory system where it has been suggested that, in addition to the firing rate, the precise timing of individual spikes is important and could contain relevant odorant information (Laurent, 1999; Wehr and Laurent, 1996). Thus, calcium imaging at a high acquisition rate (Bullen and Saggau, 1999; Iyer *et al.*, 2006; Takashima *et al.*,

1999) could serve as a powerful tool to investigate spatial patterns as well as temporal coding and would further improve our understanding of the detailed mechanisms of information processing in the olfactory bulb.

The dendrodendritic signaling between mitral and granule cells is one of the most important steps of information processing in the olfactory bulb. The mechanisms underlying the function of the mitral-granule dendrodendritic reciprocal synapses have drawn much interest and led to many studies in an attempt to characterize these synapses. However, recent studies also point out the difficulties in studying the dendrodendritic synapses by making paired recordings between synaptically coupled mitral and granule cells because of the low success rate in finding such couples (Murphy *et al.*, 2005).

Using combined CCD imaging and electrophysiological recording, we propose a possibility to record the post-synaptic events in GCs while imaging AP-correlated $[Ca^{2+}]_i$ increases in a large number of mitral cells. By correlating post-synaptic events with pre-synaptic action potentials, we could identify synaptically coupled pairs out of a large number of recorded cells. This experimental design would systematically speed up the process of recognizing coupled mitral and granule cells, which is unacceptably time-consuming if randomly picking up one cell in the mitral cell layer and then trying to find a connected one in the granule cell layer. Thus, simultaneous CCD imaging and electrical recording appears to be promising for searching and probing the neuronal connectivity of this network.

5. Summary

The olfactory bulb is the first relay stage that processes input from the sensory periphery and relays the information to many high-ordered cortical regions. Despite stimulus activity has been observed *in vivo*, to study the mechanisms underlying odor-evoked activities is much more difficult using *in vivo* preparation. In this thesis, we use a nose-olfactory bulb slice preparation of *Xenopus laevis* tadpoles and focus on characterized odor-induced spiking and $[Ca^{2+}]_i$ activities of OB neurons in the preparation.

Using loose-seal, on-cell patch-clamp recordings, we first investigate spiking activities in mitral cells (MCs) and granule cells (GCs). Both types of neurons can generate action potentials (APs) spontaneously. While a majority of MCs fire APs in bursts, the firing pattern of most GCs appeared to be random discharge. Upon odorant stimulation, spontaneous spiking activity of MCs can be modulated as inhibition or excitation. Spontaneous spikes were clearly suppressed by odorant stimulation in some MCs while odor elicits a train of spikes in other responding MCs. In contrast to MCs, most GCs generated only a few spikes during odorant stimulation.

To further reveal currents and subthreshold membrane potentials underlying the observed spiking activities, we perform patch clamp recordings in the whole-cell, voltage- and current-clamp configuration. Some MCs show an odor-induced slow inward current and APs superimposed on a subthreshold membrane potential depolarization while others display a slow outward current and an odor-induced hyperpolarization associated with odorant stimuli. In contrast to these slow synaptic currents in MCs, odorant stimulation induced a barrage of fast EPSCs in a majority of responding GCs.

These results suggest that electrical responses in MCs are driven by certain slow synaptic inputs whereas odor-evoked excitation in GCs is triggered mainly by fast excitatory inputs.

To characterize the stimulus response distributed in the olfactory bulb, we used calcium imaging to monitor activities of a large population of bulbar neurons. First, we observed prominent ongoing $[Ca^{2+}]_i$ fluctuations in most MCs and in a majority of GCs. These $[Ca^{2+}]_i$ fluctuations are dependent on the extracellular calcium influx because they can be blocked by superfusion of calcium-free external solution. Furthermore, these spontaneous fluctuations are suppressed by TTX and cadmium indicating that this $[Ca^{2+}]_i$ activity is dependent on voltage-activated sodium and calcium channels.

Odorant stimulation can modulate ongoing $[Ca^{2+}]_i$ activities of MCs as enhancement, suppression, or a combination of both, resulting in various complex $[Ca^{2+}]_i$ response waveforms in MCs. Conversely, a majority of GCs show single or compound $[Ca^{2+}]_i$ transients upon odorant stimulation. Prominent inhibitory responses in MCs indicate that MCs are functionally coupled to an intrabulbar inhibitory network.

Regarding the spatial pattern of odorant responses to a mixture of amino acids, MCs with similar response properties have certain tendency to be located in spatial neighborhood but at the same time extensively intermingle with cells of opposite response characteristics.

Finally, combining calcium imaging and on-cell patch clamp recordings, we investigated the relationship between somatic $[Ca^{2+}]_i$ and action potentials in MCs and GCs. Simultaneous recording revealed a precise correlation between $[Ca^{2+}]_i$ increases and the occurrence of spikes during spontaneous and odor-evoked activity in mitral cells. Interestingly, $[Ca^{2+}]_i$ decreases induced by odorant stimulation coincided with the suppression of the

spontaneous firing. Granule cells, however, showed much lower correlation between $[Ca^{2+}]_i$ and APs. In addition to AP-correlated $[Ca^{2+}]_i$ increases, we also observed substantial numbers of uncorrelated events such as increases of $[Ca^{2+}]_i$ without the presence of APs or APs without $[Ca^{2+}]_i$ increases. The results indicate that the relationship between somatic $[Ca^{2+}]_i$ and APs is different in mitral and granule cells. Thus, one must consider the diversity of neurons when relating $[Ca^{2+}]_i$ activity to spike activity.

6. Reference

Ache,B.W. and J.M.Young. 2005. Olfaction: diverse species, conserved principles. *Neuron* 48:417-430.

Adams,W.B. and I.B.Levitan. 1985. Voltage and ion dependences of the slow currents which mediate bursting in Aplysia neurone R15. *J Physiol* 360:69-93.

Bardoni,R., P.C.Magherini, and O.Belluzzi. 1995. Sodium current in periglomerular cells of frog olfactory bulb in vitro. *Brain Res* 703:19-25.

Bischofberger,J. and P.Jonas. 1997. Action potential propagation into the presynaptic dendrites of rat mitral cells. *J Physiol* 504:359-365.

Bootman,M.D., P.Lipp, and M.J.Berridge. 2001. The organisation and functions of local Ca(2+) signals. *J Cell Sci* 114:2213-2222.

Breer,H. 2003. Olfactory receptors: molecular basis for recognition and discrimination of odors. *Anal Bioanal Chem* 377:427-433.

Bruce,HM. 1959. An exteroceptive block to pregnancy in the mouse. *Nature* 184:105

Bullen,A. and P.Saggau. 1999. High-speed, random-access fluorescence microscopy: II. Fast quantitative measurements with voltage-sensitive dyes. *Biophys J* 76:2272-2287.

Cang,J. and J.S.Isaacson. 2003. In vivo whole-cell recording of odor-evoked synaptic transmission in the rat olfactory bulb. *J Neurosci* 23:4108-4116.

Carleton,A., L.T.Petreanu, R.Lansford, A.Alvarez-Buylla, and P.M.Lledo. 2003.

Becoming a new neuron in the adult olfactory bulb. *Nat Neurosci* 6:507-518.

Carlsson,M.A., P.Knusel, P.F.Verschure, and B.S.Hansson. 2005. Spatio-temporal Ca2+ dynamics of moth olfactory projection neurones. *Eur J Neurosci* 22:647-657.

Chen,T.W., B.J.Lin, E.Brunner, and D.Schild. 2006. In-situ background estimation in quantitative fluorescence imaging. *Biophys J*. 90:2534-2547

Chen,W.R., J.Midtgaard, and G.M.Shepherd. 1997. Forward and backward propagation of dendritic impulses and their synaptic control in mitral cells. *Science* 278:463-467.

Chen,W.R., W.Xiong, and G.M.Shepherd. 2000. Analysis of relations between NMDA receptors and GABA release at olfactory bulb reciprocal synapses. *Neuron* 25:625-633.

Chivers,DP., EL.Wildy, JM.Kiesecker, AR.Blaustein. 2001. Avoidance response of juvenile Pacific treefrogs to chemical cues of introduced predatory bullfrogs. *J Chem Ecol* 27:1667-76

Czesnik,D., L.Nezlin, J.Rabba, B.Muller, and D.Schild. 2001. Noradrenergic modulation of calcium currents and synaptic transmission in the olfactory bulb of Xenopus laevis tadpoles. *Eur J Neurosci* 13:1093-1100.

Czesnik,D., W.Rossler, F.Kirchner, A.Gennerich, and D.Schild. 2003. Neuronal representation of odourants in the olfactory bulb of Xenopus laevis tadpoles. *Eur J Neurosci* 17:113-118.

Dacey,D.M. 1996. Circuitry for color coding in the primate retina. *Proc Natl Acad Sci U S A* 93:582-588.

Denk,W., R.Yuste, K.Svoboda, and D.W.Tank. 1996. Imaging calcium dynamics in dendritic spines. *Curr Opin Neurobiol* 6:372-378.

Didier,A., A.Carleton, J.G.Bjaalie, J.D.Vincent, O.P.Ottersen, J.Storm-Mathisen, and P.M.Lledo. 2001. A dendrodendritic reciprocal synapse provides a recurrent excitatory connection in the olfactory bulb. *Proc Natl Acad Sci U S A* 98:6441-6446.

Dohlman,H.G., J.Thorner, M.G.Caron, and R.J.Lefkowitz. 1991. Model systems for the study of seven-transmembrane-segment receptors. *Annu Rev Biochem* 60:653-688.

Egger,V., K.Svoboda, and Z.F.Mainen. 2003. Mechanisms of lateral inhibition in the olfactory bulb: efficiency and modulation of spike-evoked calcium influx into granule cells. *J Neurosci* 23:7551-7558.

Egger,V., K.Svoboda, and Z.F.Mainen. 2005. Dendrodendritic synaptic signals in olfactory bulb granule cells: local spine boost and global low-threshold spike. *J Neurosci* 25:3521-3530.

Friedrich,R.W. and S.I.Korsching. 1997. Combinatorial and chemotopic odorant coding in the zebrafish olfactory bulb visualized by optical imaging. *Neuron* 18:737-752.

Friedrich,R.W. and G.Laurent. 2001. Dynamic optimization of odor representations by slow temporal patterning of mitral cell activity. *Science* 291:889-894.

Fujita,I., M.Satou, and K.Ueda. 1988. Morphology of physiologically identified mitral cells in the carp olfactory bulb: a light microscopic study after intracellular staining with horseradish peroxidase. *J Comp Neurol* 267:253-268.

Grubb,M.S. and I.D.Thompson. 2004. The influence of early experience on the development of sensory systems. *Curr Opin Neurobiol* 14:503-512.

Grynkiewicz,G., M.Poenie, and R.Y.Tsien. 1985. A new generation of Ca2+ indicators with greatly improved fluorescence properties. *J Biol Chem* 260:3440-3450.

Hartmann,J. and A.Konnerth. 2005. Determinants of postsynaptic Ca2+ signaling in Purkinje neurons. *Cell Calcium* 37:459-466.

Hayar,A., S.Karnup, M.T.Shipley, and M.Ennis. 2004. Olfactory bulb glomeruli: external tufted cells intrinsically burst at theta frequency and are entrained by patterned olfactory input. *J Neurosci* 24:1190-1199.

Hayar,A., M.T.Shipley, and M.Ennis. 2005. Olfactory bulb external tufted cells are synchronized by multiple intraglomerular mechanisms. *J Neurosci* 25:8197-8208.

Heinbockel,T., P.Heyward, F.Conquet, and M.Ennis. 2004. Regulation of main olfactory bulb mitral cell excitability by metabotropic glutamate receptor mGluR1. *J Neurophysiol* 92:3085-3096.

Hille,B. 2001. Ionic Channels in Excitable Membranes. 3nd ed. Sinauer Associates, Inc. Sunderland, MA. 814 pp.

Hirsch,J.A. 2003. Synaptic physiology and receptive field structure in the early visual pathway of the cat. *Cereb Cortex* 13:63-69.

Ikegaya,Y., G.Aaron, R.Cossart, D.Aronov, I.Lampl, D.Ferster, and R.Yuste. 2004. Synfire chains and cortical songs: temporal modules of cortical activity. *Science* 304:559-564.

Isaacson,J.S. and G.J.Murphy. 2001. Glutamate-mediated extrasynaptic inhibition: direct coupling of NMDA receptors to Ca(2+)-activated K+ channels. *Neuron* 31:1027-1034.

Isaacson,J.S. and B.W.Strowbridge. 1998. Olfactory reciprocal synapses: dendritic signaling in the CNS. *Neuron* 20:749-761.

Iyer,V., T.M.Hoogland, and P.Saggau. 2006. Fast functional imaging of single neurons using random-access multiphoton (RAMP) microscopy. *J Neurophysiol* 95:535-545.

Jiang,T. and A.Holley. 1992. Morphological variations among output neurons of the olfactory bulb in the frog (Rana ridibunda). *J Comp Neurol* 320:86-96.

Katz,L.C., C.D.Gilbert, and T.N.Wiesel. 1989. Local circuits and ocular dominance columns in monkey striate cortex. *J Neurosci* 9:1389-1399.

Kauer,J.S. 1974. Response patterns of amphibian olfactory bulb neurones to odour stimulation. *J Physiol* 243:695-715.

Kossel,A., S.Lowel, and J.Bolz. 1995. Relationships between dendritic fields and functional architecture in striate cortex of normal and visually deprived cats. *J Neurosci* 15:3913-3926.

Kovalchuk,Y., J.Eilers, J.Lisman, and A.Konnerth. 2000. NMDA receptor-mediated subthreshold Ca(2+) signals in spines of hippocampal neurons. *J Neurosci* 20:1791-1799.

Kramer,R.H. and R.S.Zucker. 1985. Calcium-induced inactivation of calcium current causes the inter-burst hyperpolarization of Aplysia bursting neurones. *J Physiol* 362:131-160.

Kuba,K., M.Nohmi, and S.Y.Hua. 1992. Intracellular Ca2+ dynamics in response to Ca2+ influx and Ca2+ release in autonomic neurones. *Can J Physiol Pharmacol* 70 Suppl:S64-S72.

Laurent,G. 1999. A systems perspective on early olfactory coding. *Science* 286:723-728.

Liljelund,P., J.G.Netzeband, and D.L.Gruol. 2000. L-Type calcium channels mediate calcium oscillations in early postnatal Purkinje neurons. *J Neurosci* 20:7394-7403.

Lin,d.Y., S.Z.Zhang, E.Block, and L.C.Katz. 2005. Encoding social signals in the mouse main olfactory bulb. *Nature* 434:470-477.

Lowe,G. 2002. Inhibition of backpropagating action potentials in mitral cell secondary dendrites. *J Neurophysiol* 88:64-85.

Lubke,J., A.Roth, D.Feldmeyer, and B.Sakmann. 2003. Morphometric analysis of the columnar innervation domain of neurons connecting layer 4 and layer 2/3 of juvenile rat barrel cortex. *Cereb Cortex* 13:1051-1063.

Maher,B.J. and G.L.Westbrook. 2005. SK channel regulation of dendritic excitability and dendrodendritic inhibition in the olfactory bulb. *J Neurophysiol* 94:3743-3750.

Mao,B.Q., F.Hamzei-Sichani, D.Aronov, R.C.Froemke, and R.Yuste. 2001. Dynamics of spontaneous activity in neocortical slices. *Neuron* 32:883-898.

Markram,H., P.J.Helm, and B.Sakmann. 1995. Dendritic calcium transients evoked by single back-propagating action potentials in rat neocortical pyramidal neurons. *J Physiol* 485 (Pt 1):1-20.

McCormick,D.A., F.Trent, and A.S.Ramoa. 1995. Postnatal development of synchronized network oscillations in the ferret dorsal lateral geniculate and perigeniculate nuclei. *J Neurosci* 15:5739-5752.

Meister,M., R.O.Wong, D.A.Baylor, and C.J.Shatz. 1991. Synchronous bursts of action potentials in ganglion cells of the developing mammalian retina. *Science* 252:939-943.

Montoro,R.J. and R.Yuste. 2004. Gap junctions in developing neocortex: a review. *Brain Res Brain Res Rev* 47:216-226.

Murphy,G.J., D.P.Darcy, and J.S.Isaacson. 2005. Intraglomerular inhibition: signaling mechanisms of an olfactory microcircuit. *Nat Neurosci* 8:354-364.

Naus,C.C. and M.Bani-Yaghoub. 1998. Gap junctional communication in the developing central nervous system. *Cell Biol Int* 22:751-763.

Nezlin,L.P. and D.Schild. 2000. Structure of the olfactory bulb in tadpoles of Xenopus laevis. *Cell Tissue Res* 302:21-29.

Niell,C.M. and S.J.Smith. 2005. Functional imaging reveals rapid development of visual response properties in the zebrafish tectum. *Neuron* 45:941-951.

Nieuwkoop,P.D., and J.Faber. 1956. Normal tables of *Xenopus laevis* (Daudin). Amsterdam: North-Holland.

Ohki,K., S.Chung, Y.H.Ch'ng, P.Kara, and R.C.Reid. 2005. Functional imaging with cellular resolution reveals precise micro-architecture in visual cortex. *Nature* 433:597-603.

Pearl,CA., M.Cervantes, M.Chan, U.Ho, R.Shoji, EO.Thomas. 2000. Evidence for a

mate-attracting chemosignal in the dwarf African clawed frog Hymenochirus. *Horm Behav* 38:67-74

Pinault,D. 1996. A novel single-cell staining procedure performed in vivo under electrophysiological control: Morpho-functional features of juxtacellularly labeled thalamic cells and other central neurons with biocytin or Neurobiotin. *Journal of Neuroscience Methods* 65:113-136.

Puopolo,M., B.P.Bean, and E.Raviola. 2005. Spontaneous activity of isolated dopaminergic periglomerular cells of the main olfactory bulb. *J Neurophysiol* 94:3618-3627.

Ressler,K.J., S.L.Sullivan, and L.B.Buck. 1994a. A molecular dissection of spatial patterning in the olfactory system. *Curr Opin Neurobiol* 4:588-596.

Ressler,K.J., S.L.Sullivan, and L.B.Buck. 1994b. Information coding in the olfactory system: evidence for a stereotyped and highly organized epitope map in the olfactory bulb. *Cell* 79:1245-1255.

Robert,C., V.Tseeb, C.Kordon, and C.Hammond. 1999. Patch-clamp-induced perturbations of [Ca(2+)](i) activity in somatotropes. *Neuroendocrinology* 70:343-352.

Rospars,J.P., P.Lansky, J.Vaillant, P.Duchamp-Viret, and A.Duchamp. 1994. Spontaneous activity of first- and second-order neurons in the frog olfactory system. *Brain Res* 662:31-44.

Satou,M. 1990. Synaptic organization, local neuronal circuitry, and functional segregation of the teleost olfactory bulb. *Prog Neurobiol* 34:115-142.

Scalia,F., G.Gallousis, and S.Roca. 1991. A note on the organization of the amphibian

olfactory bulb. *J Comp Neurol* 305:435-442.

Schild,D. 1985. A Computer-Controlled Device for the Application of Odors to Aquatic Animals. *Journal of Electrophysiological Techniques* 12:71-79.

Schoppa,N.E., J.M.Kinzie, Y.Sahara, T.P.Segerson, and G.L.Westbrook. 1998. Dendrodendritic inhibition in the olfactory bulb is driven by NMDA receptors. *J Neurosci* 18:6790-6802.

Shepherd,G.M. 1972. Synaptic organization of the mammalian olfactory bulb. *Physiol Rev* 52:864-917.

Shipley,M.T. and M.Ennis. 1996. Functional organization of olfactory system. *J Neurobiol* 30:123-176.

Smetters,D., A.Majewska, and R.Yuste. 1999. Detecting action potentials in neuronal populations with calcium imaging. *Methods* 18:215-221.

Stocker,M. and P.Pedarzani. 2000. Differential distribution of three Ca(2+)-activated K(+) channel subunits, SK1, SK2, and SK3, in the adult rat central nervous system. *Mol Cell Neurosci* 15:476-493.

Stosiek,C., O.Garaschuk, K.Holthoff, and A.Konnerth. 2003. In vivo two-photon calcium imaging of neuronal networks. *Proc Natl Acad Sci U S A* 100:7319-7324.

Sullivan,M.R., A.Nimmerjahn, D.V.Sarkisov, F.Helmchen, and S.S.Wang. 2005. In vivo calcium imaging of circuit activity in cerebellar cortex. *J Neurophysiol* 94:1636-1644.

Takami,S. and P.P.Graziadei. 1990. Morphological complexity of the glomerulus in

the rat accessory olfactory bulb--a Golgi study. *Brain Res* 510:339-342.

Takami,S. and P.P.Graziadei. 1991. Light microscopic Golgi study of mitral/tufted cells in the accessory olfactory bulb of the adult rat. *J Comp Neurol* 311:65-83.

Takashima,I., M.Ichikawa, and T.Iijima. 1999. High-speed CCD imaging system for monitoring neural activity in vivo and in vitro, using a voltage-sensitive dye. *J Neurosci Methods* 91:147-159.

Vassar,R., S.K.Chao, R.Sitcheran, J.M.Nunez, L.B.Vosshall, and R.Axel. 1994. Topographic organization of sensory projections to the olfactory bulb. *Cell* 79:981-991.

Verkhratsky,A.J. and O.H.Petersen. 1998. Neuronal calcium stores. *Cell Calcium* 24:333-343.

Wang,X., J.S.McKenzie, and R.E.Kemm. 1996. Whole cell calcium currents in acutely isolated olfactory bulb output neurons of the rat. *J Neurophysiol* 75:1138-1151.

Wang,Y., H.F.Guo, T.A.Pologruto, F.Hannan, I.Hakker, K.Svoboda, and Y.Zhong. 2004. Stereotyped odor-evoked activity in the mushroom body of Drosophila revealed by green fluorescent protein-based Ca2+ imaging. *J Neurosci* 24:6507-6514.

Waters,J., M.Larkum, B.Sakmann, and F.Helmchen. 2003. Supralinear Ca2+ influx into dendritic tufts of layer 2/3 neocortical pyramidal neurons in vitro and in vivo. *J Neurosci* 23:8558-8567.

Wehr,M. and G.Laurent. 1996. Odour encoding by temporal sequences of firing in

oscillating neural assemblies. *Nature* 384:162-166.

Wong,A.M., J.W.Wang, and R.Axel. 2002. Spatial representation of the glomerular map in the Drosophila protocerebrum. *Cell* 109:229-241.

Woolf,T.B., G.M.Shepherd, and C.A.Greer. 1991. Local information processing in dendritic trees: subsets of spines in granule cells of the mammalian olfactory bulb. *J Neurosci* 11:1837-1854.

Xiong,W. and W.R.Chen. 2002. Dynamic gating of spike propagation in the mitral cell lateral dendrites. *Neuron* 34:115-126.

Yamada,S., H.Takechi, I.Kanchiku, T.Kita, and N.Kato. 2004. Small-conductance Ca2+-dependent K+ channels are the target of spike-induced Ca2+ release in a feedback regulation of pyramidal cell excitability. *J Neurophysiol* 91:2322-2329.

Yokoi,M., K.Mori, and S.Nakanishi. 1995. Refinement of odor molecule tuning by dendrodendritic synaptic inhibition in the olfactory bulb. *Proc Natl Acad Sci U S A* 92:3371-3375.

Yu,C.R., J.Power, G.Barnea, S.O'Donnell, H.E.Brown, J.Osborne, R.Axel, and J.A.Gogos. 2004. Spontaneous neural activity is required for the establishment and maintenance of the olfactory sensory map. *Neuron* 42:553-566.

Yunker,A.M., A.H.Sharp, S.Sundarraj, V.Ranganathan, T.D.Copeland, and M.W.McEnery. 2003. Immunological characterization of T-type voltage-dependent calcium channel CaV3.1 (alpha 1G) and CaV3.3 (alpha 1I) isoforms reveal differences in their localization, expression, and neural development. *Neuroscience* 117:321-335.

Yuste,R. and L.C.Katz. 1991. Control of postsynaptic Ca2+ influx in developing neocortex by excitatory and inhibitory neurotransmitters. *Neuron* 6:333-344.

Yuste,R., D.A.Nelson, W.W.Rubin, and L.C.Katz. 1995. Neuronal domains in developing neocortex: mechanisms of coactivation. *Neuron* 14:7-17.

Yuste,R., A.Peinado, and L.C.Katz. 1992. Neuronal domains in developing neocortex. *Science* 257:665-669.

Zelles,T., J.D.Boyd, A.B.Hardy, and K.R.Delaney. 2006. Branch-specific Ca2+ influx from Na+-dependent dendritic spikes in olfactory granule cells. *J Neurosci* 26:30-40.

Zippel, H.P., and W.Breipohl. 1975. Functions of the olfactory system in the goldfish (*Carassius auratus*). Denton, D.A. and J.P.Coghlan. eds. Olfaction and Taste V. New York: Academic Press, pp. 163-167.

7. Acknowledgements

The deepest thank goes to Prof. Schild for his fully supporting me and my work from various kinds of aspects.

I would like to thank my PhD committee members, Prof. Stuehmer and Prof. Fuchs for their helpful advice and suggestions to my work.

I also want to thank Prof. Hoerner for his taking care of us and the neuroscience program.

Thanks then go to all the professors and tutors I met in the first year of the neuroscience course. Thank you for introducing me many interesting thoughts and perspectives about neuroscience.

I would specially thank members of the Department of Neurophysiology and Cellular Biophysics, Dr. Ivan Manzini, Dr. Dirk Czesnik, Dr. Friedrich Kirchner, Gudrun Federkeil, Stefanie Ludwig, Josko Kuduz, Dr. Andre Zeug, Dr. Gaudin Arnaud Christian Michael, Eugen Kludt, Stephan Junek, Arwed Wiegel, Daniel Governatori, Benjamin Gutermann, Cristoph Brase, Johannes Roettger, Saskia Schweer, Johannes Richter, Silvia Kurtanska, Franziska Ulmer for their constant help throughout my work and many special moments with you together.

Thanks also go to all my colleagues of the neuroscience program. Without you, the life won’t be so active.

Last but not least, I want to thank Tsai-Wen for all his help and for the share of every feeling with me.

8. Curriculum vitae

Bei-Jung Lin

born: 06/15/1977 in Taipei, Taiwan

Scientific training:

1995-1999	Department of Zoology, National Taiwan University, Taiwan
1999	B.S. National Taiwan University,
1999-2001	Institute of Physiology, College of Medicine, National Taiwan University
2000-2001	Master student in the lab of Prof. Chung-Chin Kuo, Cellular Electrophysiology Laboratory, Institute of Physiology, College of Medicine, National Taiwan University
2001/06	M.S. College of Medicine, National Taiwan University
2001/10	Student of International Program of Neuroscience, Goettingen, Germany
2002/08	Admission to the PhD program in International

Neuroscience Program, Goettingen, Germany

Awards and Scholarships:

1995,1996	President Awards of National Taiwan University
1997	College Student Research Scholarship of National Science Council, Taiwan
2002/10	Goerg-Christoph-Lichtenberg Stipendiums, Niedersachsen State, Germany

Publication List:

Lin, B.J., T.W. Chen and D. Schild. Spontaneous and odor-modulated calcium activities in the olfactory bulb and their correlation with electrical activities. *In preparation.*

Chen,T.W., B.J.Lin, E.Brunner, and D.Schild. 2006. In situ background estimation in quantitative fluorescence imaging. *Biophys J* 90:2534-2547

Kuo,C.C., B.J.Lin, H.R.Chang, and C.P.Hsieh. 2004. Use-dependent inhibition of the N-methyl-D-aspartate currents by felbamate: a gating modifier with selective binding to the desensitized channels. *Mol Pharmacol* 65:370-380.